

การใช้ปริมาณรังสีอย่างเหมาะสมสำหรับเครื่องซีที 320 สไลซ์ โดยการปรับค่าพีทซ์และเทคนิค  
การปรับกระแสหลอด-เวลาเพื่อให้ได้ค่าเบี่ยงเบนมาตรฐานที่เหมาะสมบนภาพที่มีคุณภาพยอมรับ  
ได้ของก้อนเนื้อในปอดโดยใช้โปรโตคอลทรวงอก: การศึกษาในหุ่นจำลอง



นางสาวฉัตรนภา นันตื้อ

จุฬาลงกรณ์มหาวิทยาลัย

CHULALONGKORN UNIVERSITY

วิทยานิพนธ์นี้เป็นส่วนหนึ่งของการศึกษาตามหลักสูตรปริญญาวิทยาศาสตรมหาบัณฑิต

สาขาวิชาฉายาเวชศาสตร์ ภาควิชารังสีวิทยา

คณะแพทยศาสตร์ จุฬาลงกรณ์มหาวิทยาลัย

ปีการศึกษา 2556

ลิขสิทธิ์ของจุฬาลงกรณ์มหาวิทยาลัย

บทคัดย่อและแฟ้มข้อมูลฉบับเต็มของวิทยานิพนธ์ตั้งแต่ปีการศึกษา 2554 ที่ให้บริการในคลังปัญญาจุฬาฯ (CUIR)

เป็นแฟ้มข้อมูลของนิสิตเจ้าของวิทยานิพนธ์ ที่ส่งผ่านทางบัณฑิตวิทยาลัย

The abstract and full text of theses from the academic year 2011 in Chulalongkorn University Intellectual Repository (CUIR)  
are the thesis authors' files submitted through the University Graduate School.

OPTIMIZATION OF 320 MDCT USING BEAM PITCH AND TUBE CURRENT  
MODULATION FOR PROPER TARGET SD ON LUNG NODULE –CHEST PROTOCOL:  
PHANTOM STUDY

Miss Chatnapa Nuntue



จุฬาลงกรณ์มหาวิทยาลัย

CHULALONGKORN UNIVERSITY

A Thesis Submitted in Partial Fulfillment of the Requirements  
for the Degree of Master of Science Program in Medical Imaging

Department of Radiology

Faculty of Medicine

Chulalongkorn University

Academic Year 2013

Copyright of Chulalongkorn University

Thesis Title	OPTIMIZATION OF 320 MDCT USING BEAM PITCH AND TUBE CURRENT MODULATION FOR PROPER TARGET SD ON LUNG NODULE –CHEST PROTOCOL: PHANTOM STUDY
By	Miss Chatnapa Nuntue
Field of Study	Medical Imaging
Thesis Advisor	Associate Professor Anchali Krisanachinda, Ph.D.
Thesis Co-Advisor	Kitiwat Khamwan, Ph.D.

---

Accepted by the Faculty of Medicine, Chulalongkorn University in Partial Fulfillment of the Requirements for the Master's Degree

.....Dean of the Faculty of Medicine  
(Associate Professor Sophon Napathorn, M.D.)

THESIS COMMITTEE

.....Chairman  
(Assistant Professor Nitra Piyavisetpat, M.D.)

.....Thesis Advisor  
(Associate Professor Anchali Krisanachinda, Ph.D.)

.....Thesis Co-Advisor  
(Kitiwat Khamwan, Ph.D.)

.....External Examiner  
(Professor Franco Milano, Ph.D.)

ฉัตรนภา นันตื้อ : การใช้ปริมาณรังสีอย่างเหมาะสมสำหรับเครื่องซีที 320 สไลซ์ โดยการปรับค่าพิทช์และเทคนิคการปรับกระแสหลอด-เวลาเพื่อให้ได้ค่าเบี่ยงเบนมาตรฐานที่เหมาะสมบนภาพที่มีคุณภาพยอมรับได้ของก้อนเนื้อในปอดโดยใช้โปรโตคอลทรวงอก: การศึกษาในหุ่นจำลอง. (OPTIMIZATION OF 320 MDCT USING BEAM PITCH AND TUBE CURRENT MODULATION FOR PROPER TARGET SD ON LUNG NODULE –CHEST PROTOCOL: PHANTOM STUDY) อ.ที่ปรึกษาวิทยานิพนธ์หลัก: รศ. ดร. อัญชลี กฤษณจินดา, อ.ที่ปรึกษาวิทยานิพนธ์ร่วม: อ. ดร. กิติวัฒน์ คำวัน, 96 หน้า.

วิธีลดปริมาณรังสีใช้เทคนิคการปรับค่ากระแสหลอด-วินาที และค่าเบี่ยงเบนมาตรฐานเป็นส่วนหนึ่งของระบบควบคุมปริมาณรังสีแบบอัตโนมัติจากเครื่องเอกซเรย์คอมพิวเตอร์ชนิด 320 สไลซ์ ซึ่งโรงงานผู้ผลิตใช้ค่าเบี่ยงเบนมาตรฐานในการควบคุมคุณภาพของภาพโดยควบคุมสัญญาณรบกวนบนภาพและเกี่ยวข้องกับปริมาณรังสีที่ผู้ป่วยได้รับ งานวิจัยนี้มีวัตถุประสงค์เพื่อประเมินปริมาณรังสีและคุณภาพของภาพเมื่อมีการตั้งค่าเบี่ยงเบนมาตรฐาน และค่าพิทช์ที่ต่างกัน และหาค่าเบี่ยงเบนมาตรฐาน และค่าพิทช์ที่เหมาะสม โดยศึกษาในหุ่นจำลองทรวงอกและก้อนเนื้อในปอด

หุ่นจำลองทรวงอกภายในมีก้อนเนื้อรูปทรงกลม 5 ก้อน ขนาดเส้นผ่าศูนย์กลาง 12, 10, 8, 5 และ 3 มม. ถูกนำมาสแกนด้วยเครื่องเอกซเรย์คอมพิวเตอร์ ด้วยการตั้งค่าพารามิเตอร์ที่แตกต่างกันของค่าพิทช์ 3 ค่า คือ 0.637, 0.813 และ 1.388, ค่าความต่างศักย์หลอดเอกซเรย์ คือ 120 และ 100, ค่าเบี่ยงเบนมาตรฐาน 9, 14, 20, 25 และค่ากระแสหลอดต่ำที่สุดถึงสูงที่สุดคือ 10-400 มิลลิแอมแปร์ ทำการบันทึกค่าปริมาณรังสี ชนิด C\_VOL และ DLP จากหน้าจอ ประเมินคุณภาพของภาพเชิงปริมาณโดยวิธีการหาอัตราส่วนความคมชัดของภาพต่อสัญญาณรบกวน (ซีเอ็นอาร์) การประเมินในเชิงคุณภาพโดยความสามารถในการแสดงก้อนเนื้อทรงกลมจำลอง และขนาดของก้อนเนื้อทรงกลมจำลองที่เล็กที่สุดโดยรังสีแพทย์ 2 คน

จากผลการศึกษาพบว่าเมื่อมีการใช้ค่าเบี่ยงเบนมาตรฐาน และค่าพิทช์ที่แตกต่างกันสำหรับเครื่องเอกซเรย์คอมพิวเตอร์ชนิด 320 สไลซ์ด้วยหุ่นจำลองทรวงอกและก้อนเนื้อในปอด ค่า C\_VOL ลดลงจาก 5.9 เหลือ 0.7 มิลลิเกรย์ สำหรับค่าความต่างศักย์หลอดเอกซเรย์ 120 และลดลงจาก 5.3 เหลือ 0.8 มิลลิเกรย์ สำหรับค่าความต่างศักย์หลอดเอกซเรย์ที่ 100 ค่า C\_VOL และ DLP ของค่าความต่างศักย์หลอดเอกซเรย์ 120 สูงกว่าค่าความต่างศักย์หลอดเอกซเรย์ 100 เล็กน้อยในทุกค่าพิทช์ และค่าเบี่ยงเบนมาตรฐาน 9 และ 14 แต่สำหรับค่าเบี่ยงเบนมาตรฐาน 20 และ 25 ค่า C\_VOL ไม่เปลี่ยนแปลงในทุกค่าพิทช์ ค่าพิทช์ 0.637 ให้ค่าเปอร์เซ็นต์ซีเอ็นอาร์มากที่สุด ค่าเปอร์เซ็นต์ซีเอ็นอาร์ของ lung window มีค่าสูงกว่าค่าเปอร์เซ็นต์ซีเอ็นอาร์ของ soft tissue window ในพิทช์ทุกค่า และยังให้ค่าขนาดของก้อนเนื้อทรงกลมจำลองที่เล็กที่สุดอีกเช่นกัน การให้คะแนนในการประเมินคุณภาพของภาพโดยรังสีแพทย์ 2 คนอยู่ในเกณฑ์ดี

ปัจจัยที่ส่งผลต่อปริมาณรังสี คือ ค่าเบี่ยงเบนมาตรฐาน และค่าความต่างศักย์หลอดเอกซเรย์ ส่วนปัจจัยที่ส่งผลต่อคุณภาพของภาพ ได้แก่ ค่าเบี่ยงเบนมาตรฐาน ค่าพิทช์ และค่าความต่างศักย์หลอดเอกซเรย์ การพิจารณาใช้ค่าเบี่ยงเบนมาตรฐานขึ้นอยู่กับพยาธิสภาพของโรคปอด จากผลการศึกษาสามารถสรุปได้ว่า การตรวจเนื้อเยื่อปอดโดยโปรโตคอลที่เหมาะสมใช้ค่าเบี่ยงเบนมาตรฐาน 20 ค่ากระแสหลอด 10-400 มิลลิแอมแปร์ ค่าพิทช์ 0.813 และค่าความต่างศักย์หลอดเอกซเรย์ 120

ภาควิชา รังสีวิทยา

ลายมือชื่อนิสิต .....

สาขาวิชา ฉายาเวชศาสตร์

ลายมือชื่อ อ.ที่ปรึกษาวิทยานิพนธ์หลัก .....

ปีการศึกษา 2556

ลายมือชื่อ อ.ที่ปรึกษาวิทยานิพนธ์ร่วม .....

# # 5574117930 : MAJOR MEDICAL IMAGING

KEYWORDS: TARGET SD / AUTOMATIC EXPOSURE CONTROL / LUNG NODULE / BEAM PITCH

CHATNAPA NUNTUE: OPTIMIZATION OF 320 MDCT USING BEAM PITCH AND TUBE CURRENT MODULATION FOR PROPER TARGET SD ON LUNG NODULE –CHEST PROTOCOL: PHANTOM STUDY. ADVISOR: ASSOC. PROF. ANCHALI KRISANACHINDA, Ph.D., CO-ADVISOR: KITIWAT KHAMWAN, Ph.D., 96 pp.

Tube current modulation is one of the radiation dose reduction methods. Target SD is a part of AEC system designed by the manufacturer to select the image quality by fixing the image noise and be able to reduce the radiation dose. The purposes of this study are to determine the radiation dose and image quality when varying Target SD and beam pitch. Optimal protocols are obtained by the appropriate Target SD and beam pitch using lung man phantom with nodules.

The lung man chest phantom with five spheres simulated nodules of 12, 10, 8, 5 and 3 mm diameters at 100 HU were scanned with varying beam pitch of 0.637, 0.813, 1.388, kVp at 120 and 100, Target SD from 9 to 25 and mA of 10-400 for 320 MDCT. The radiation dose in term of C\_VOL (mGy) and DLP (mGy.cm) were recorded from the CT monitor. The quantitative image quality was determined by the contrast to noise ratio (CNR) values, the qualitative image quality was evaluated in part of spatial resolution and nodule detection capability by two independent radiologists.

When varying Target SD and beam pitch for 320 MDCT using lung man phantom and nodules, C\_VOL decreased from 5.9 to 0.7 mGy for 120 kVp and 5.3 to 0.8 mGy for 100 kVp. The C\_VOL and DLP of 120 kVp were slightly higher than at 100 kVp in all pitch on Target SD 9 and 14 but for Target SD 20 and 25, C\_VOL did not change in all pitch. The percent CNR is highest at pitch 0.637 when compared to other pitch. The percent CNR of lung window is higher than soft tissue window for all pitch and the best spatial resolution image was also obtained with lung window. The scoring on image quality by two radiologists was in good agreement.

Target SD and kVp affect radiation dose while Target SD, pitch and kVp affect the image quality. The selection Target SD depends on clinical applications. Optimal protocol for routine chest CT is Target SD 20, 10-400 mA at pitch 0.813 and 120 kVp.

Department: Radiology

Field of Study: Medical Imaging

Academic Year: 2013

Student's Signature .....

Advisor's Signature .....

Co-Advisor's Signature .....

## ACKNOWLEDGEMENTS

I would like to express my gratitude and deepest appreciation to Associate Professor Anchali Krisanachinda, Ph.D., Department of Radiology, Faculty of Medicine, Chulalongkorn University, my advisor for her helpful, suggestion, supervision, guidance, constructive direction and polishing of the thesis to improve English expression.

I would like to express my thankfulness to Mr. Kitiwat Khamwan, Ph.D., Department of Radiology, Faculty of Medicine, Chulalongkorn University, my co-advisor for his helpful, suggestion, guidance and polishing of the thesis writing to improve the English expression.

I would like to deeply thank Assistant Professor Nitra Piyavisetpat, M.D., Department of Radiology, Faculty of Medicine, Chulalongkorn University, Chairperson of thesis defense and Professor Franco Milano, Ph.D., University of Florence Italy, External examiner for their kind suggestion and constructive comments in this research.

I am extremely grateful to Associate Professor Sivalee Suriyapee, Chief Physicist at Division of Radiation Oncology, Department of Radiology, Faculty of Medicine, Chulalongkorn University, for her invaluable guidance, constructive direction and encouragement.

I would like to truly thank Ms. Thanisa Tongbai, M.D., Ms. Patcharee Hongsmatip, M.D., Department of Radiology, Faculty of Medicine, Chulalongkorn University, for their kind evaluation on image quality in this research.

I would like to thank Mrs. Petcharleeya Suwanpradit and Mrs. Walaiporn Suksancharoen, Medical Physicist and technologist at the Unit of Computed Tomography, King Chulalongkorn Memorial Hospital, for their guidance on CT scanner, kindly support and useful advice.

I am greatly grateful for all teachers, lecturers and staff at Master of Science Program in Medical Imaging, Faculty of Medicine, Chulalongkorn University for their suggestions and teaching during the course of Medical Imaging.

Finally, I am heartfelt thankful to my family for their invaluable encouragement, entirely care, financial support and understanding during the entire course of the study.

## CONTENTS

	Page
THAI ABSTRACT .....	iv
ENGLISH ABSTRACT .....	v
ACKNOWLEDGEMENTS .....	vi
CONTENTS .....	vii
LIST OF TABLES .....	xi
LIST OF FIGURES.....	xiii
LIST OF ABBREVIATIONS .....	xvii
CHAPTER I INTRODUCTION .....	1
1.1 Background and Rationale .....	1
1.2 Research objectives.....	3
1.3 Definition .....	3
CHAPTER II REVIEW OF RELATED LITERATURE .....	4
2.1 Theory .....	4
2.1.1 The introduction of Computed Tomography .....	4
2.1.2 Multi Detector CT (MDCT).....	4
2.1.3 Image reconstruction .....	5
2.1.4 Hounsfield Unit or CT number.....	7
2.1.5 Window Width (WW) and Window Level (WL).....	7
2.1.6 Computed Tomography Dose Index (CTDI).....	8
2.1.6.1 $C_{PMMA,100}$ .....	8
2.1.6.2 Weighted CT Dose Index ( $C_w$ ).....	9
2.1.6.3 Volume CT Dose Index ( $C_{VOL}$ ).....	9
2.1.6.4 Dose-Length Product (DLP).....	9
2.1.7 Beam Pitch .....	10
2.1.8 Image quality .....	10
2.1.8.1 Spatial resolution.....	10
2.1.8.2 Contrast resolution.....	11

	Page
2.1.8.3 Image noise.....	11
2.1.9 Automatic exposure control (AEC).....	12
2.1.9.1 Z-axis modulation.....	12
2.1.9.2 Angular dose modulation.....	13
2.1.9.3 Target SD.....	13
2.2 Review related literature.....	14
CHAPTER III RESEARCH METHODOLOGY.....	16
3.1 Research design.....	16
3.2 Research design model.....	16
3.3 Conceptual framework.....	17
3.4 Research question.....	17
3.5 Materials.....	18
3.5.1 CT scanner, Toshiba Aquilion ONE.....	18
3.5.2 Lung man chest phantom study.....	18
3.5.3 Simulated lung nodules.....	19
3.5.4 Catphan <sup>®</sup> 600 phantom.....	19
3.5.5 PMMA phantom.....	20
3.5.6 Unfors model Xi base unit with mAs display.....	21
3.5.7 CT pencil-type ionization chamber.....	21
3.6 Methods.....	22
3.6.1 Perform the quality control of Toshiba Aquilion ONE.....	22
3.6.2 Verification of $C_{a, 100}$ .....	22
3.6.3 Verification of $C_{VOL}$ .....	22
3.6.4 Image quality in Catphan phantom.....	23
3.6.4.1 High contrast resolution.....	23
3.6.4.2 Contrast to noise ratio.....	23
3.6.5 Phantom study.....	24



	Page
3.6.6 Optimization of the radiation dose and image quality .....	26
3.7 Data analysis .....	27
3.8 Sample size determination .....	28
3.9 Statistical analysis .....	28
3.10 Outcome measurement .....	28
3.11 Ethical consideration .....	28
3.12 Expected benefit .....	29
CHAPTER IV RESULTS .....	30
4.1 Quality control of the CT scanner: TOSHIBA Aquilion ONE .....	30
4.2 Verification of Computed Tomography Dose Index (CTDI) .....	31
4.2.1 Measurement CT air kerma index ( $C_{a,100}$ ) .....	31
4.2.2 $C_{PMMA,100}$ in head phantom .....	33
4.2.3 $C_{PMMA, 100}$ in body phantom .....	34
4.2.4 $C_{VOL}$ on monitor and calculated $C_w$ .....	35
4.2.5 The measured $C_{VOL}$ of monitor and calculated $C_w$ compared with IEC values for 120 kVp .....	37
4.3 Characteristic of image quality in Catphan phantom .....	38
4.3.1 Contrast to Noise Ratio .....	38
4.3.2 Spatial resolution .....	39
4.4 Radiation dose .....	40
4.5 Image quality .....	44
4.5.1 Quantitative image quality .....	44
4.5.1.1 Contrast to Noise Ratio (CNR) .....	44
4.5.2 Qualitative image quality .....	70
4.5.2.1 Image scoring .....	70
4.5.2.2 Spatial resolution .....	70
CHAPTER V DISCUSSION AND CONCLUSIONS .....	72
5.1 Discussion .....	72

	Page
5.1.1 Measurement of CTDI .....	72
5.1.2 Radiation dose, pitch and Target SD.....	72
5.1.2.1 The assessment of image quality.....	73
5.1.2.1.1 Contrast to Noise Ratio .....	73
5.1.2.1.2 The assessment of qualitative image quality .....	74
5.1.2.2 Optimization of radiation dose, image quality, Target SD and pitch .....	74
5.2 Conclusions.....	76
REFERENCES .....	77
Appendix A: Data record form .....	81
Appendix B: Quality Control of MDCT system .....	85
VITA.....	96

## LIST OF TABLES

	Page
<b>Table 3. 1</b> The five point scale for image quality.....	27
<b>Table 4. 1</b> Report of CT system performance.....	30
<b>Table 4. 2</b> The measured $C_{a,100}$ in air for head protocols for each kVp and slice collimations. ....	31
<b>Table 4. 3</b> The measured $C_{a,100}$ in air for body protocol for each kVp and slice collimation. ....	32
<b>Table 4. 4</b> The measured $C_{PMMA,100}$ at each position of head phantom for each kVp, $C_w$ and $nC_w$ in unit of mGy/mAs.....	33
<b>Table 4. 5</b> The measured $C_{PMMA,100}$ at each position of body phantom for each kVp, $C_w$ and $nC_w$ in unit of mGy/mAs.....	34
<b>Table 4. 6</b> $C_{VOL}$ displayed on monitor and calculated $C_w$ using head techniques 100 mAs and 240 mm FOV, slice collimation 4x4 mm .....	35
<b>Table 4. 7</b> $C_{VOL}$ displayed on monitor and calculated $C_w$ using body techniques 100 mAs and 400 mm FOV(L) slice collimation 4x4 mm.....	36
<b>Table 4. 8</b> The measured $C_{VOL}$ of monitor and calculated $C_w$ compared with IEC values using head technique 100 mA, 1-s, Scan field: S (240 mm) 4 mm x 4 slice thickness.....	37
<b>Table 4. 9</b> The measured $C_{VOL}$ of monitor and calculated $C_w$ compared with IEC values using body technique 100 mA, 1-s, Scan field: L (400 mm) 4 mm x 4 slice thickness.....	38
<b>Table 4. 10</b> The measured of CT number (HU) of low contrast object and background values and calculate CNR of Catphan phantom.....	38
<b>Table 4. 11</b> Spatial resolution.....	39
<b>Table 4. 12</b> $C_{VOL}$ , DLP of Lung man phantom at 120 kVp.....	40
<b>Table 4. 13</b> $C_{VOL}$ , DLP of Lung man phantom at 100 kVp.....	41
<b>Table 4. 14</b> The percent $C_{VOL}$ reduction with increasing Target SD from 9 to 25 and increasing pitch at 120 kVp.....	42
<b>Table 4. 15</b> The percent $C_{VOL}$ reduction with increasing Target SD from 9 to 25 and increasing pitch at 100 kVp.....	43

<b>Table 4. 16</b>	The percent CNR of nodule 12 mm in diameter for soft tissue window	45
<b>Table 4. 17</b>	The percent CNR of nodule 10 mm in diameter for soft tissue window	46
<b>Table 4. 18</b>	The percent CNR of nodule 8 mm in diameter for soft tissue window ..	47
<b>Table 4. 19</b>	The percent CNR of nodule 5 mm in diameter for soft tissue window ..	48
<b>Table 4. 20</b>	The percent CNR of nodule 3 mm in diameter for soft tissue window ..	49
<b>Table 4. 21</b>	The percent CNR of nodule 12 mm in diameter for lung window.....	50
<b>Table 4. 22</b>	The percent CNR of nodule 10 mm in diameter for lung window.....	51
<b>Table 4. 23</b>	The percent CNR of nodule 8 mm in diameter for lung window .....	52
<b>Table 4. 24</b>	The percent CNR of nodule 5 mm in diameter for lung window .....	53
<b>Table 4. 25</b>	The percent CNR of nodule 3 mm in diameter for lung window .....	54
<b>Table 4. 26</b>	The image scoring of Lung man chest phantom with soft tissue window .....	70
<b>Table 4. 27</b>	The image scoring of Lung man chest phantom with lung window. ....	70
<b>Table 4. 28</b>	The spatial resolution of Lung man chest phantom at 100 and 120 kVp .....	71
<b>Table B 1:</b>	Alignment of table and bore.....	86
<b>Table B 2:</b>	Table increment Accuracy .....	86
<b>Table B 3:</b>	The accuracy of slice separation.....	87
<b>Table B 4:</b>	The accuracy of gantry angle tilt.....	88
<b>Table B 5:</b>	Reproducibility of CT Number .....	88
<b>Table B 6:</b>	mGy and mAs linearity .....	89
<b>Table B 7:</b>	Linearity of CT Number .....	90
<b>Table B 8:</b>	Accuracy of Distance Measurement.....	92
<b>Table B 9:</b>	High contrast resolution .....	93
<b>Table B 10:</b>	Low contrast detectability.....	94
<b>Table B 11:</b>	Slice thickness accuracy.....	94
<b>Table B 12:</b>	Image Uniformity .....	95

## LIST OF FIGURES

	Page
<b>Figure 2. 1</b> Different detector array used in multiple-row detector CT scanners .....	5
<b>Figure 2. 2</b> Process involved in CT image reconstruction .....	6
<b>Figure 2. 3</b> The relationship between spatial resolution and image noise of different convolution kernel.....	6
<b>Figure 2. 4</b> The Hounsfield scale of CT numbers.....	7
<b>Figure 2. 5</b> The radiation dose profile along the z-axis on single section .....	8
<b>Figure 2. 6</b> The concepts of beam pitch .....	10
<b>Figure 2. 7</b> Automatic tube current control in CT (a) in different patient size; (b) along the patient's long axis; and (c) throughout a gantry rotation .....	12
<b>Figure 2. 8</b> Angular modulation of tube current is performed at different projections in the x-y plane within each 360° x-ray tube rotation.....	13
<b>Figure 3. 1</b> 320 detector row CT Toshiba Aquilion ONE scanner.....	18
<b>Figure 3. 2</b> Lung man chest phantom .....	18
<b>Figure 3. 3</b> Simulated lung nodule of sphere 12, 10, 8, 5 and 3 mm in diameters ...	19
<b>Figure 3. 4</b> Catphan <sup>®</sup> 600 Phantom .....	20
<b>Figure 3. 5</b> Cylindrical PMMA phantom of 16 and 32 cm diameters .....	20
<b>Figure 3. 6</b> Unfors Raysafe model Xi base unit with mAs display .....	21
<b>Figure 3. 7</b> 10 cm length of the pencil-type ionization Unfors Xi CT Detector .....	21
<b>Figure 3. 8</b> Measurement the CT number of low contrast object and background....	24
<b>Figure 3. 9</b> The location of simulated nodules.....	24
<b>Figure 3. 10</b> Measurement the CT number of nodule and background.....	26
<b>Figure 4. 1</b> $C_{a,100}$ in air, head protocol as the function of kVp and slice collimation are plotted in blue, red, green and violet colors at kVp of 80, 100, 120 and 135 respectively.....	32
<b>Figure 4. 2</b> $C_{a,100}$ in air, body protocol as the function of kVp and slice collimation are plotted in blue, red, green and violet colors of kVp 80, 100, 120 and 135 respectively. ....	33
<b>Figure 4. 3</b> $C_{VOL}$ (mGy) and $C_w$ (mGy) of head phantom as the function of kVp are plotted in red (measured) and blue (displayed) straight lines of less than 10 percent discrepancy.....	36

<b>Figure 4. 4</b> $C_{VOL}$ (mGy) and $C_w$ (mGy) of body phantom as the function of kVp are plotted red (measured) and blue (displayed) straight lines of less than 10 percent discrepancy.....	37
<b>Figure 4. 5</b> Measurement the CT number of low contrast object and background....	39
<b>Figure 4. 6</b> Spatial resolution part of Catphan phantom .....	40
<b>Figure 4. 7</b> The relationship between $C_{VOL}$ and Target SD with different pitch at 120 kVp.....	41
<b>Figure 4. 8</b> The relationship between $C_{VOL}$ and Target SD with different pitch at 100 kVp.....	42
<b>Figure 4. 9</b> The relationship between DLP and Target SD with different pitch at 120 kVp.....	43
<b>Figure 4. 10</b> The relationship between DLP and Target SD with different pitch at 100 kVp.....	44
<b>Figure 4. 11</b> The percent CNR of nodule 12 mm, at 120 (a) and 100 kVp (b) for soft tissue window.....	55
<b>Figure 4. 12</b> The percent CNR of nodule 10 mm, at 120 (a) and 100 kVp (b) for soft tissue window.....	55
<b>Figure 4. 13</b> The percent CNR of nodule 8 mm, at 120 (a) and 100 kVp (b) for soft tissue window.....	56
<b>Figure 4. 14</b> The percent CNR of nodule 5 mm, at 120 (a) and 100 kVp (b) for soft tissue window.....	56
<b>Figure 4. 15</b> The percent CNR of nodule 3 mm, at 120 (a) and 100 kVp (b) for soft tissue window.....	57
<b>Figure 4. 16</b> The percent CNR of nodule 12 mm, at 120 (a) and 100 kVp (b) for lung window .....	57
<b>Figure 4. 17</b> The percent CNR of nodule 10 mm, at 120 (b) and 100 kVp (b) for lung window .....	58
<b>Figure 4. 18</b> The percent CNR of nodule 8 mm, at 120 (a) and 100 kVp (b) for lung window .....	58

<b>Figure 4. 19</b> The percent CNR of nodule 5 mm, at 120 (a) and 100 kVp (b) for lung window .....	59
<b>Figure 4. 20</b> The percent CNR of nodule 3 mm, at 120 (a) and 100 kVp (b) for lung window .....	59
<b>Figure 4. 21</b> The percent CNR of nodule 12 mm, at 120 kVp compared between soft tissue window and lung window for pitch 0.637 (a), pitch 0.813 (b) and pitch 1.388 (c) .....	60
<b>Figure 4. 22</b> The percent CNR of nodule 10 mm, at 120 kVp compared between soft tissue window and lung window for pitch 0.637 (a), pitch 0.813 (b) and pitch 1.388 (c) .....	61
<b>Figure 4. 23</b> The percent CNR of nodule 8 mm, at 120 kVp compared between soft tissue window and lung window for pitch 0.637 (a), pitch 0.813 (b) and pitch 1.388 (c) .....	62
<b>Figure 4. 24</b> The percent CNR of nodule 5 mm, at 120 kVp compared between soft tissue window and lung window for pitch 0.637 (a), pitch 0.813 (b) and pitch 1.388 (c) .....	63
<b>Figure 4. 25</b> The percent CNR of nodule 3 mm, at 120 kVp compared between soft tissue window and lung window for pitch 0.637 (a), pitch 0.813 (b) and pitch 1.388 (c) .....	64
<b>Figure 4. 26</b> The percent CNR of nodule 12 mm, at 100 kVp compared between soft tissue window and lung window for pitch 0.637 (a), pitch 0.813 (b) and pitch 1.388 (c) .....	65
<b>Figure 4. 27</b> The percent CNR of nodule 10 mm, at 100 kVp compared between soft tissue window and lung window for pitch 0.637 (a), pitch 0.813 (b) and pitch 1.388 (c) .....	66
<b>Figure 4. 28</b> The percent CNR of nodule 8 mm, at 100 kVp compared between soft tissue window and lung window for pitch 0.637 (a), pitch 0.813 (b) and pitch 1.388 (c) .....	67

<b>Figure 4. 29</b> The percent CNR of nodule 5 mm, at 100 kVp compared between soft tissue window and lung window for pitch 0.637 (a), pitch 0.813 (b) and pitch 1.388 (c) .....	68
<b>Figure 4. 30</b> The percent CNR of nodule 3 mm, at 100 kVp compared between soft tissue window and lung window for pitch 0.637 (a), pitch 0.813 (b) and pitch 1.388 (c) .....	69
<b>Figure 5. 1</b> The chest CT with 5 mm nodule with soft tissue window (a) and lung window (b), Target SD 20, 10-400 mA, pitch 0.813 and 120 kVp.....	75
<b>Figure B 1</b> The relationship of mGy/mAs and mAs.....	90
<b>Figure B 2</b> Linearity of CT number .....	91
<b>Figure B 3</b> Distance accuracy.....	91
<b>Figure B 4</b> High contrast resolution.....	92
<b>Figure B 5</b> Low contrast detectability.....	93
<b>Figure B 6</b> Image Uniformity .....	95



## LIST OF ABBREVIATIONS

Abbreviation	Terms
3D	Three dimensions
AEC	Automatic exposure control
cm	centimeter
cm <sup>3</sup>	Cubic centimeter
C <sub>a,100</sub>	CT air kerma index measure free in air integrated over 100 mm
CNR	Contrast to noise ratio
C <sub>PMMA,100</sub>	Computed tomography dose index measure with the standard CT dosimetry phantom
CT	Computed tomography
CTDI	Computed tomography dose index
C <sub>VOL</sub>	Volume computed tomography dose index
C <sub>w</sub>	Weighted computed tomography dose index
DLP	Dose-Length Product
FOV	Field of view
GGOs	Ground-glass opacities
GGA	Ground-glass attenuation
HRCT	High contrast resolution computed tomography
HU	Hounsfield unit
Kg	Kilo gram
kVp	Kilo voltage peak
kW	Kilo watt
Lp/cm	Line pairs per centimeter
mA	Milliampere
mAs	Milliampere-second
MDCT	Multi-detector computed tomography
μGy	MicroGray
mGy	MilliGray

Abbreviation	Terms
mGy.cm	Milligray-centimeter
MHU	Mega heat unit
mm	Millimeter
MTF	Modulation transfer function
mSv	MilliSievert
PMMA	Polymethylmethacrylate
ROI	Region of interest
s	Second
SD	Standard deviation
Target SD	Target standard deviation
WW	Window width
WL	Window level

# CHAPTER I

## INTRODUCTION

### 1.1 Background and Rationale

Since the beginning of clinical application of MDCT in the late 1990s, MDCT has played a very important role in routine clinical practices. This has raised concerns because of the associated radiation exposure and its potential link to induction of cancer. The contribution of CT examinations to the collective dose from diagnostic radiation exposure is estimated to be 67% in the United States and 47% in the United Kingdom[1]. The potential radiation risk from this increased use of CT makes it important that CT doses should be kept as low as reasonably achievable.

In addition, academic and social interested in radiation dose reduction for CT examinations without any decrease in diagnostic capability has been growing. The issue of radiation dose reduction is currently drawing widespread attention. In the last decade, dose reduction strategies have been realized by using various techniques, such as tube current reduction, tube voltage reduction, scan length optimization, scan protocol individualization, noise reduction filters, iterative reconstructions and utilization of automatic exposure control (AEC). Moreover, there are several scan features also effect on radiation dose that operator cannot change such as scanner geometry, x-ray beam filters, pre-patient tracking of x-ray tube focal spot and projection adaptive reconstruction filters.

The method with the great potential for dose reduction is the Automatic Exposure Control (AEC) or automatic tube current (mA) modulation technique. AEC is a generic name for technique which tube current is adjusted according to the patient's attenuation to reduce the radiation dose to the patient while sustaining diagnostic image quality [2]. The AEC system of Toshiba should be studied for the optimization of patient dose using tube current modulation as a function of projection angle (angular modulation), longitudinal location along the patients (z-axis modulation) or both. The image quality is specified in terms of Target standard deviation (SD), to control image noise and the tube current is adjusted to preserve the same level of noise in each image. Sure exposure, specific term for Toshiba MDCT, has been set in relation to the Target SD as the measurement of image quality [3]

As the radiation dose is inversely proportional to pitch, thus the important parameter in dose reduction protocol is pitch. In MDCT, pitch has been defined in definitions as the ratio of table feed per rotation and total collimated x-ray width (number of slices × detector collimation) [2]. In theoretical, increasing the pitch by increasing the table speed reduces the radiation dose and scanning time.

The image quality is one of the important functions of CT system. There are many factors affect the image quality such as Target SD and beam pitch. Low Target SD and beam pitch indicates higher image quality with excess radiation to patient. Conversely, high Target SD and beam pitch will result in radiation saving but they will contribute higher image noise resulting poor image quality. Another indicator of image quality in this study is the contrast to noise ratio (CNR) that related the pitch, Target SD and tube voltage (kVp).

In this study, the optimization of CT chest with lung nodules has been chosen. It is the study on anatomical region which the radiation dose could be reduced for the intrinsic contrast in the chest and lower pulmonary absorption of radiation. Currently, MDCT is a powerful modality for clinical detection of chest disease especially lung cancers at a smaller size of nodule and earlier stage compared with chest radiography. Patients checked up for lung screening and patients with the small solitary pulmonary nodules need to follow up the nodules size several times for evaluation of malignancy. In addition in female chest, breasts are radiosensitive organ that directly proportional to radiation dose. The results of this study would contribute the optimized protocol of Toshiba 320-MDCT for radiation dose and image quality to patient. Moreover, the optimization for the radiation dose and image quality is an important for the CT operator and radiologist.

## 1.2 Research objectives

1.2.1 To determine the radiation dose and image quality when varying Target SD and beam pitch in lung man phantom with nodules.

1.2.2 To obtain the appropriate Target SD and beam pitch for lung man phantom with nodules.

## 1.3 Definition

### Target SD

The technique parameter designed by the vendor to determine the noise level. It is reference to the standard deviation of pixel value of a specific-attenuation water phantom and compared to the patient's CT radiograph (Scanogram) data in order to maintain image noise.

## CHAPTER II

### REVIEW OF RELATED LITERATURE

#### 2.1 Theory

##### 2.1.1 The introduction of Computed Tomography

Computed Tomography (CT) is a medical imaging method that combines multiple x-ray projections taken from different angles to produce detailed cross-sectional images of areas inside the body. CT images present very precise, 3-D views of certain parts of the body, such as soft tissues, pelvis, blood vessels, lungs, brain, heart, abdomen and bones [4]

Early CT scanners acquired images a single slice at a time (sequential scanning). However, during the 1990s significant advancements in technology heralded the development of slip ring technology, which enabled the x-ray tube to rotate continuously in one direction around the patient. This has contributed to the development of helical or spiral CT. In spiral CT, the x-ray tube rotates continuously in one direction whilst the table on which the patient is lying is mechanically moved through the x-ray beam. The transmitted radiation thus takes on the form of a helix or spiral. Instead of acquiring data one slice at a time, information can be acquired as a continuous volume of contiguous slices. This allows larger anatomical regions of the body to be imaged during a single breath hold, thereby reducing the possibility of artifacts caused by patient movement. Faster scanning also increases patient throughput and increases the probability of a diagnostically useful scan in patients who are unable to fully cooperate with the investigation. These multi slice or multi detector machines utilize the principles of the helical scanner but incorporate multiple rows of detector rings. Thus they can acquire multiple slices per tube rotation, thereby increasing the area of the patient that can be covered in a given time by the x-ray beam [5].

##### 2.1.2 Multi Detector CT (MDCT)

Continued scanner development on the road to a 3D radiograph called for further progress. An obvious improvement would be to make more efficient use of the x rays that are produced by the tube while improving z-axis spatial resolution; this led to the development of multiple-row detector arrays. The basic idea actually dates to the very first EMI Mark I scanner, which had two parallel detectors and acquired two sections simultaneously. The first helical scanner to use this idea, the CT Twin (Elscint, Haifa, Israel), was launched in 1992. This design was advanced to single-row detector designs that all scanner manufacturers went back to the drawing board. By late 1998, all major CT manufacturers launched multiple-row detector.

CT scanners are capable of acquiring at least four sections per rotation. The arrangement of detectors along the z axis and the widths of the available sections vary between the systems. Figure 2.1 shows different multiple-row detector array configurations from several manufacturers. Current multiple-row detector scanners can scan large 40-cm volume lengths in less than 30 seconds with near-isotropic resolution and image quality that could not be envisioned at the time of Hounsfield's invention[6].

At present, CT scanner has developed rapidly. The rapid pace of developments in scanner technology over the last twenty years, especially the acceleration of development in last ten years from four to 320-slice scanner.

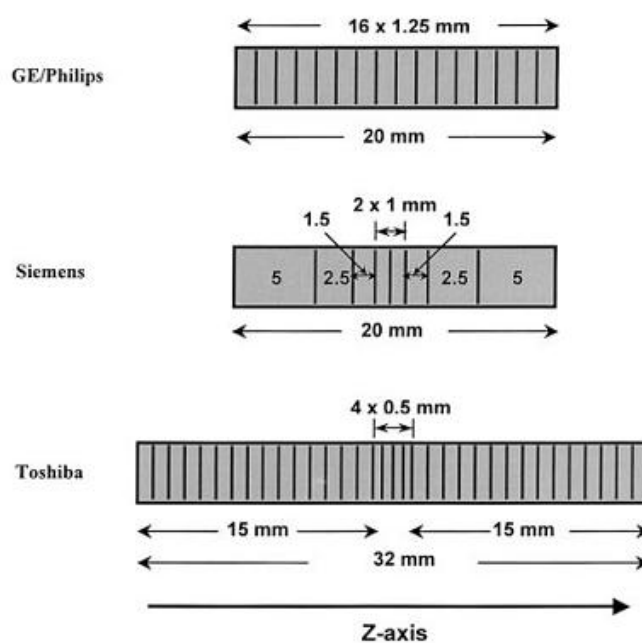


Figure 2. 1 Different detector array used in

multiple-row detector CT scanners

[6]

### 2.1.3 Image reconstruction [7]

The detector signal registered during a scan is preprocessed to compensate for inhomogeneities in the detector system and to correct for beam hardening effects within the patient. After various correction steps and transformation from signal intensities into x-ray attenuation values these data called "CT raw data" as shown in Figure 2.2

The raw data sets for third and fourth generation scanners consist of the attenuation profile of some 500 to 1200 projections for 360° rotation of the x-ray tube. Image reconstruction from the raw data sets finally yields the image data set.

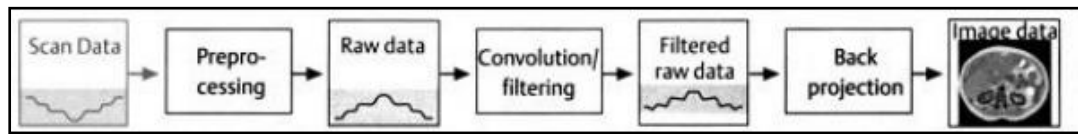


Figure 2. 2 Process involved in CT image reconstruction [7]

Image reconstruction starts with the selection of the desired field of view (FOV). Each ray from the tube to the detectors that passes through this FOV is used for reconstruction. The attenuation coefficient for each image point is determined by averaging attenuation values for all rays that cross this point (back projection). This type of unfiltered back projection yields a very unsharp image with blur edges. There for multiple rays are assembled into a projection and the resulting attenuation profile subjected to an edge enhancing mathematic filtering (convolution process).

The “convolution kernel” is usually referred to the type of filtering. The convolution kernel used for filter back projection determines the properties of reconstructed CT sections in terms of spatial resolution and image noise and can vary from soft or smooth to sharp or edge-enhancing as shown in Figure 2.3 Standard kernel is designed as suitable for a good spatial resolution and low image noise for CT applications.

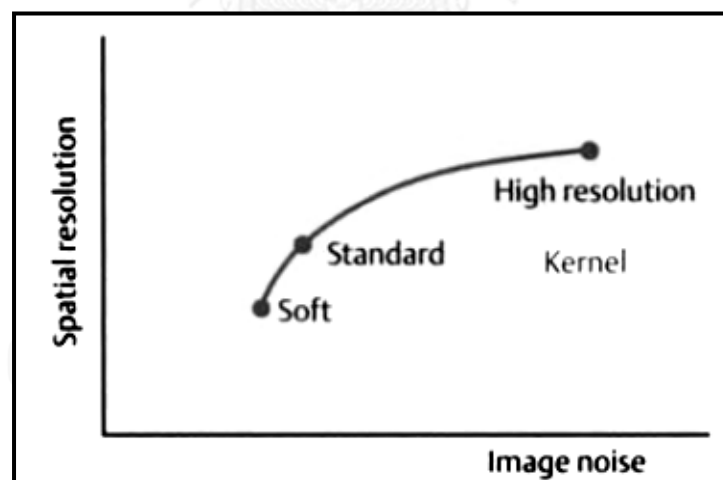


Figure 2. 3 The relationship between spatial resolution and image noise of different convolution kernel [7]



### 2.1.4 Hounsfield Unit or CT number [4]

During image reconstruction, each pixel is assigned a numerical value (CT number), which is the average of all the attenuation values contained within the corresponding voxel. The CT number or HU is defined as in equation 2.1:

$$HU = 1000 \times \frac{\mu_x - \mu_{water}}{\mu_{water}} \quad (2.1)$$

Where  $\mu_x$  is linear attenuation coefficient of voxel  $x$  and  $\mu_{water}$  is linear attenuation coefficient of water.

This number is compared to the attenuation value of water and displayed on a scale of units named Hounsfield units (HU). This scale assigns water as an attenuation value (HU) of zero. The range of CT numbers is 2000 HU wide although some modern scanners have a greater range of HU up to 4000. Each number shows a shade of grey with +1000 (white) and -1000 (black) at either end of the spectrum as shown in Figure 2.4[4]

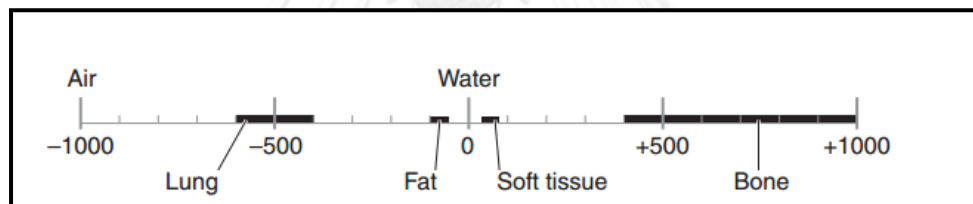


Figure 2. 4 The Hounsfield scale of CT numbers [4]

### 2.1.5 Window Width (WW) and Window Level (WL) [4]

As the range of CT numbers discriminate by the computer is 2000, the human eye cannot accurately distinguish between 2000 different shades of grey. Therefore to allow the observer to interpret the image, only a limited number of HU are displayed. A clinically useful grey scale is achieved by setting the WL and WW on the computer displayed to a suitable range of Hounsfield units, depending on the tissue being studied. The term 'window level' shows the central Hounsfield unit of all the numbers within the window width. The window width covers the HU of all the tissues of interest and these are displayed as various shades of grey. Tissues with CT numbers out of this range are shown as either black or white.

### 2.1.6 Computed Tomography Dose Index (CTDI) [8]

The CTDI is the primary dose measurement concept in CT. It represents the average dose along the z axis from series of contiguous irradiation in one axial scan or one rotation of x-ray tube within the central region of scan volume.

#### 2.1.6.1 $C_{PMMA,100}$

$C_{PMMA,100}$  represents the accumulated multiple scan dose at the center of a 100 mm scan and underestimates the accumulated dose for longer scan lengths. The  $C_{PMMA,100}$  is integration of the radiation dose profile from a single axial scan over specific integration limits and the integration limits are  $\pm 50$  mm as shown in Figure 2.5 which corresponds to the 100 mm length of the “pencil” ionization chamber. The  $C_{PMMA,100}$  is calculated as the integral of air kerma along chamber divided by nominal slice thickness as in equation 2.2

$$C_{PMMA,100} = \frac{1}{NT} \int_{-50\text{ mm}}^{50\text{ mm}} D(Z) dz \quad (2.2)$$

Where N is the number of acquire slices per rotation and T is nominal thickness of acquire slice (mm).

The use of a single, consistent integration limit to avoided the problem of dose overestimation for narrow slice widths.  $CTDI_{100}$  is acquired using a 100-mm, “pencil” ionization chamber and the two standard PMMA phantoms head (16-cm diameter) and body (32-cm diameter)

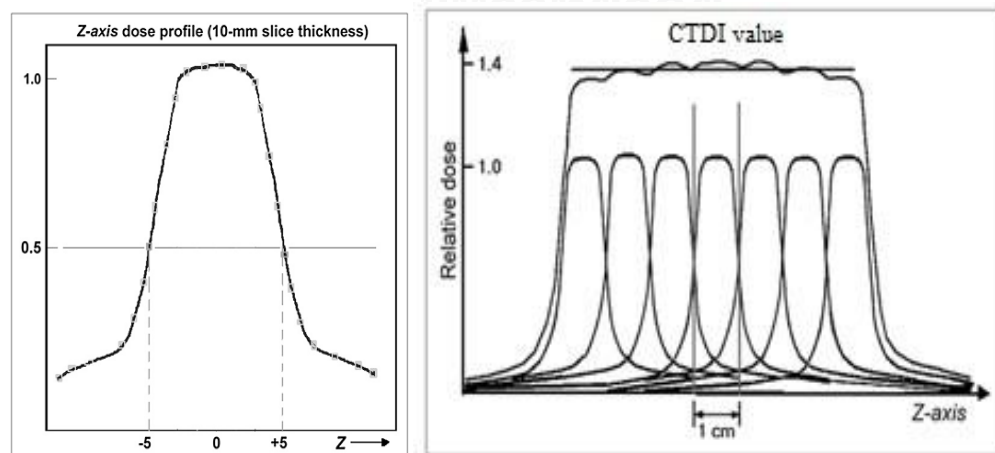


Figure 2. 5 The radiation dose profile along the z-axis on single section [9]

### 2.1.6.2 Weighted CT Dose Index ( $C_w$ )

The  $C_w$  represents average CTDI across the field of view (FOV) and useful indicator of scanner radiation output for a specific kVp and mAs. The CTDI is typically a factor or two higher at the surface than at the center of the FOV. The  $C_w$  is defined as in equation 2.3

$$C_w = \frac{1}{3} CPMMA, 100, center + \frac{2}{3} CPMMA, 100, periphery \quad (2.3)$$

The values of  $\frac{1}{3}$  and  $\frac{2}{3}$  approximate the relative areas represented by the center and periphery values.

### 2.1.6.3 Volume CT Dose Index ( $C_{VOL}$ )

The volume CT dose index provides a single CT dose parameter, based on a directly and easily measured quantity. In the unit of milligray (mGy). The  $C_{VOL}$  represents the average absorbed radiation dose over the x, y, and z directions within scan volume for standardized phantom and represent dose for a specific scan protocol, which involves a series of scans, it is essential to take into account any gaps or overlaps between the x-ray beams from consecutive rotations of the x-ray source. This is accomplished with use of a dose descriptor known as the Volume  $C_w$  ( $C_{VOL}$ ), where;

$$CVOL = \frac{N \times T}{I} \times Cw$$

Where I is the table increment per axial scan (mm), N is the number of acquire slices per rotation and T is nominal thickness of acquire slice (mm).

### 2.1.6.4 Dose-Length Product (DLP)

To better represent the overall energy delivered by a given scan protocol, the absorbed dose can be integrated along the scan length to compute the Dose-Length Product (DLP), where

$$DLP(mGy - cm) = Cvol (mGy) \times Scan length(cm)$$

The implications of overranging with regard to the DLP depends on the length of the image body region. For helical scans that are short relative to the total beam width, the dose efficiency (with regard to overranging) will decrease. For the same anatomic coverage, it is generally more dose efficient to use a single helical scan than multiple helical scans.

### 2.1.7 Beam Pitch

In MDCT, pitch has been defined in two definitions as the ratio of table feed per rotation (T) and the total collimated x-ray width (number of slices  $\times$  detector collimation) and as the ratio of table feed per rotation and the slice thickness[6] as shown in Figure 2.6 A beam pitch of 1.0 provides an acquisition with no overlap or gap, a beam-pitch of less than 1.0 provides an overlapping acquisition and higher patient dose, while a beam-pitch of greater than 1.0 provides a gap acquisition and low patient dose and image quality [3]

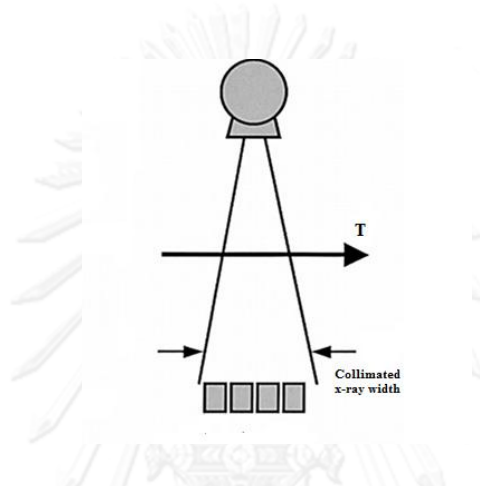


Figure 2. 6 The concepts of beam pitch [10]

The use of beam pitch is applicable equally to both single-row detector helical CT and multiple row detector CT and eliminates the confusion existing between the relationship of radiation dose and various manufacturers' defined pitch [11].

### 2.1.8 Image quality

The primary characteristics that affect the image quality in CT are spatial resolution, contrast resolution, image noise and artifacts.

#### 2.1.8.1 Spatial resolution

Spatial resolution describes the ability of an image system to accurately depict objects in the two spatial dimensions of the image. Basically, the capability of an image system to distinctly characterize of two objects as they become smaller and closer together. The ways to measure spatial resolution of an image system is high contrast test objects where signal to noise level is high and does not influence recognition. It can also be specified in terms of spatial frequency, in line pairs per cm (lp/cm), for particular levels of the modulation transfer function (MTF). The MTF measures how well an imaging system transfer information from the object to the image and expressed in percent [8].

### 2.1.8.2 Contrast resolution

Contrast resolution is the ability of a CT scanner to differentiate small attenuation differences on the CT image. Contrast Resolution is also known as low contrast resolution and tissue resolution. CT scan image tissues that vary only slightly in density and atomic number. Most soft tissues have atomic numbers or densities that are nearly the same. The ability of the CT scanner to image these slight differences is known as low contrast detectability, which is used to describe contrast resolution in computed tomography. Actually, contrast resolution describes the CT systems ability to discriminate between two or more anatomical structures that attenuate "nearly" the same amount of x-ray photons [12].

Generator power is an important factor in low contrast examinations. Low noise images require high tube current (mA) values, particularly when coupled with fast rotation speeds and narrow slice acquisitions. Fast rotation speeds decrease movement artifacts, thin slices improve spatial resolution as well as decrease partial volume effects. Dose efficiency of the scanner is a significant factor in these types of examinations, as it will evaluate the dose required to provide level of contrast resolution [13].

### 2.1.8.3 Image noise [9]

In general, noise in CT depends on the number of x-ray photons reaching the detector (quantum noise). Since x-ray photon statistics obey the Poisson distribution, quantum noise is proportional to  $\sqrt{N}$  and the corresponding image noise is inversely proportional to the square root of number of photons ( $\frac{1}{\sqrt{N}}$ ) that have contributed to the reconstructed image.

CT noise appears as fluctuations in CT numbers, a measurement of image noise is a measurement of these fluctuations, and such a measurement can be made using regions of interest (ROIs) on a scan of a uniform phantom. A statistical ROI function (available on most CT scanners) allows users to place a rectangular or oval ROI on the image, within which is calculated the average and standard deviation (SD) of the CT numbers for the enclosed pixels. The SD indicates the magnitude of random fluctuations in the CT number and thus is related to noise: The larger the SD, the higher the image noise.

The following scanner design features affect the image noise:

- Tube current: Changing the mA value changes the beam intensity, therefore affect to the number of x-ray photons.
- Slice thickness: Changing the thickness changes the x-ray beam width reaching each detector, therefore affect to the number of detected x-ray photons.

- Peak kilovoltage (kVp): Increasing the peak kilovoltage increases the number of x-rays penetrating the patient and reaching the detectors. Thus, increasing the kilovoltage reduces image noise but can (slightly) reduce subject contrast as well.

### 2.1.9 Automatic exposure control (AEC)

Automatic exposure control, the technique aims to modulate tube current on the basis of regional body anatomy for adjustment of x-ray quantum noise to maintain constant image noise with improved dose efficiency[14]. Any changes to accommodate different patient size had to be estimated and implemented manually. Modern scanners are equipped with automatic exposure control mechanisms, which adjust the tube current for changing patient attenuation throughout a scan. The adjustment can be made to compensate for changing attenuation (Figure 2.7) Most modern systems have the capability to operate all three compensation modes, which are generally implemented simultaneously [13].

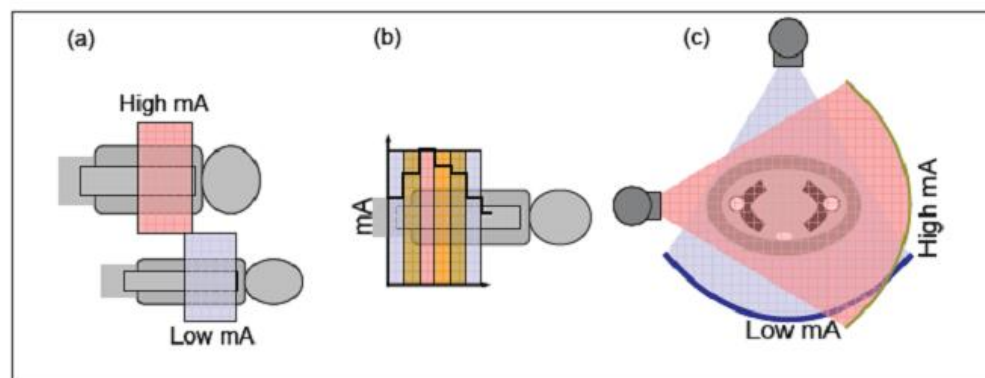


Figure 2. 7 Automatic tube current control in CT (a) in different patient size; (b)along the patient's long axis; and (c) throughout a gantry rotation [13]

#### 2.1.9.1 Z-axis modulation [2]

Scan projection radiographs (topographic views) are applied in patient-size, used mainly for evaluation of the size and attenuation of the patient. In reality, AEC systems tend to operate on the basis of a single anteroposterior topographic view to achieve compatibility with existing clinical practice. The aim of z-axis modulation is to reduce the variation in the quality of images from the same series. Z-axis modulation determines the tube current on the basis of projection data obtained from a topogram and a set of empirically determined noise prediction coefficients with use of the reference technique. These projection data can be used to determine the attenuation, size, and shape of the patient.

### 2.1.9.2 Angular dose modulation [2]

Angular dose modulation involves varying the tube current to adjust the photon flux to the detector as the x-ray tube rotates about the patient. This technique makes use of the data obtained from two topograms (anteroposterior and lateral views). With this data, sinusoidal modulation of tube current is achieved during 360° rotation for compensation of x-ray absorption. In a noncircular cross-sectional geometry, attenuation varies in different projection angles. At angular projections with a small patient diameter or body region, the tube current can be reduced without significantly increasing the image noise as shown in Figure 2.8. Generally, lateral projections are more attenuating than anteroposterior projections. In angular dose modulation, more dose modulations occur in asymmetric regions and the variation in image noise throughout the examination can be minimized. This rotational AEC is also helpful in reducing photon starvation artifacts, especially in the shoulder.

CT equipment manufacturers always provide AEC systems with a combination of two of these types of AEC. Most MDCT now perform these AEC systems, which include near real-time modulation techniques requiring x-ray tubes and generators to vary their output rapidly for sub second rotation times.

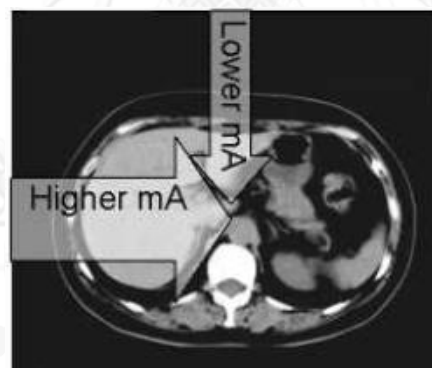


Figure 2. 8 Angular modulation of tube current is performed at different projections in the x-y plane within each 360° x-ray tube rotation [2]

### 2.1.9.3 Target SD [15]

The Toshiba Aquilion One scanner presents both longitudinal (z-axis) and angular modulation (x-axis, y-axis) automatic tube current modulation. This modulation adjusts tube current to maintain as user defined Target SD (noise level) in the image data that is essentially independent of patient size and anatomy. The Target SD value is calculating from the “water-equivalent” thickness of each section from the localizer radiograph. The appropriate tube current

is applied at the thickest section to achieve the selected standard deviation (noise level). Tube current is then modulated to maintain the selected noise level throughout the entire scan.

## 2.2 Review related literature

**Keiko Matsumoto, et al [16] reported** ‘3D automatic exposure control for 64-detector row CT: Radiation dose reduction in chest phantom study’. The objective was to determine the utility of three-dimensional (3D) automatic exposure control (AEC) for low-dose CT examination in a chest phantom study. A chest CT phantom with simulated focal ground-glass opacities (GGOs) and nodules was scanned with a 64-detector row CT with and without AEC. Performance of 3D AEC included changing targeted standard deviations (SDs) of image noise from scout view to assess the appropriate targeted SD (40-150) for identification GGOs and nodules. The capability of overall identification with the CT protocol adapted to each of the targeted SDs was compared with that obtained with CT without AEC by means of receiver operating characteristic (ROC) analysis. The results showed a targeted SD of 150 were to be used for nodule identification with the low-dose CT protocol using AEC and the radiation dose could be reduced by almost 75% as compared with standard-dose CT without significant degradation of detection capability. These implications suggest that the most appropriate targeted SD value for 3D AEC should be chosen according to the purpose of the examination. Moreover, radiation dose reduction can be expected to vary according to the purpose of the examination.

**Yoshiharu Ohno, et al. [17] reported** ‘Influence of detector collimation and beam pitch for identification and image quality of ground-glass attenuation and nodules on 16-and 64-detector row CT systems: Experimental study using chest phantom’. The objective was to determine the influence of detector collimation and beam pitch for identification and image quality of ground-glass attenuation (GGA) and nodules on 16- and 64-detector row CTs, by using a chest phantom. Chest CT phantom that simulated the GGAs and nodules was scanned with two different MDCT scanners including thin and thick collimated examination protocols with comparable beam pitch and tube current settings and with consecutive thin image reconstruction, and lung window setting. The probability of each simulated abnormality was visually assessed with a five-point scoring system. The results showed that the radiation dose for 16- and 64-detector row CTs reduced to almost 15% compared with standard CT protocols. The image quality of low-dose CT for any MDCT system is significantly different from the standard chest CT protocol (p-value <0.05). They found that the beam pitch is influenced on the detectability of simulated GGAs and nodules, and recommended. For low-dose CT protocol with a thin detector collimation a low-beam should be used for further reduction of tube current and radiation dose with 16-and 64-detector row CT systems.

**J. D. Silverman, et al [18] reported** ‘Investigation of lung nodule detectability in low-dose 320-slice computed tomography’. The objective was to determine the extent to which radiation dose can be minimized while maintaining diagnostic performance through



knowledgeable selection of reconstruction techniques. A 320- MDCT scanner was used to scan an anthropomorphic phantom with combination of kVp and mAs at doses ranging from 0.1 mGy (80 kVp, 3.5 mAs) to 12.5 mGy (120 kVp, 105 mAs) . Detectability of a small solid lung nodule (3.2 mm diameter, -37 HU) was determined as a function of dose and reconstruction filter including smooth soft-tissue filters, smooth filter with proprietary noise reduction and sharp filter with slice thickness. The results indicated that radiation dose can be reduced below the current low-dose (5 mGy) with knowledgeable selection of reconstruction parameters. Image noise and spatial resolution were found to be the limiting factor in detection of small lung nodules. Thus, the use of smoother reconstruction filters may permit lower-dose protocols without trade-off in diagnostic performance.

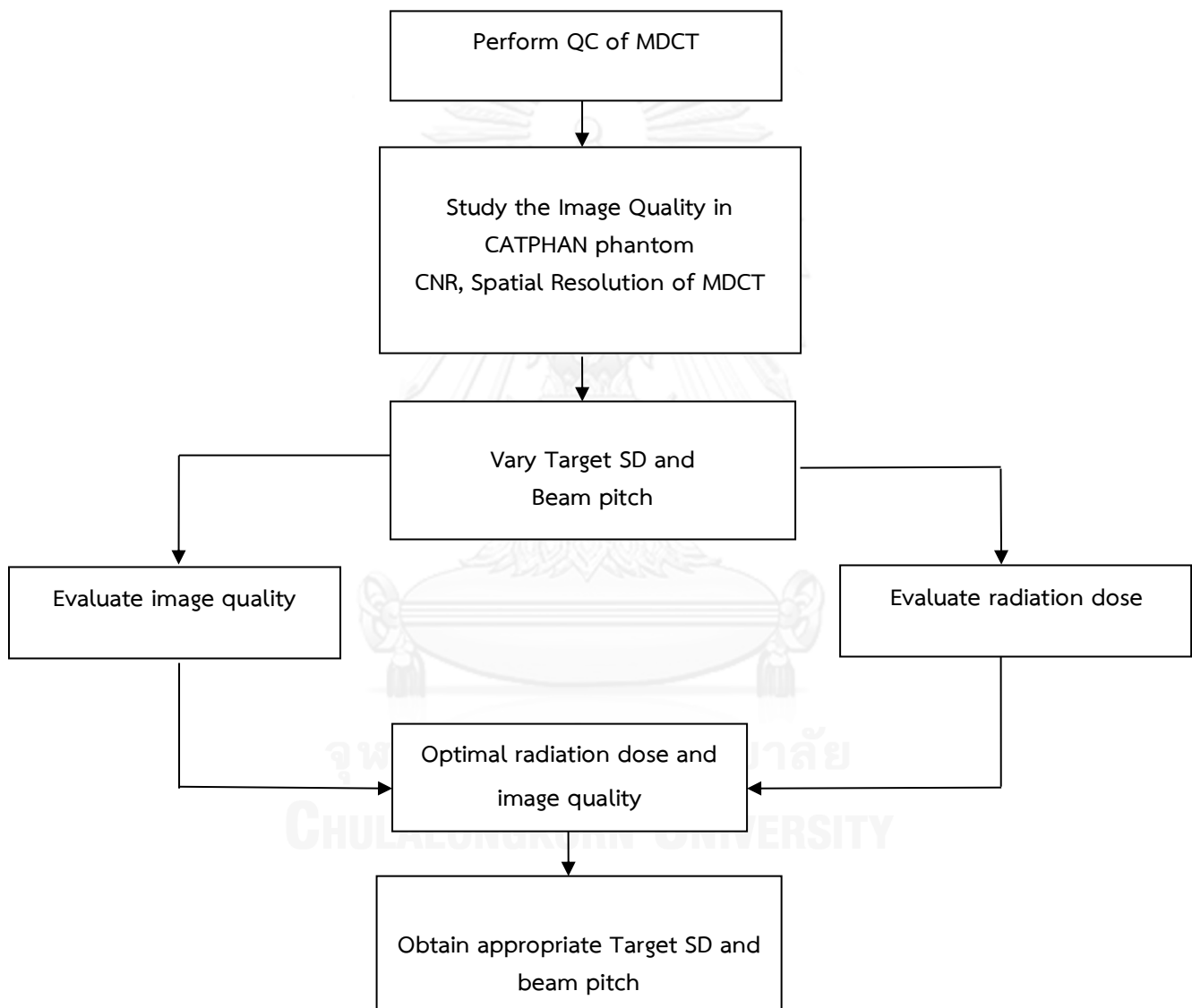


### CHAPTER III RESEARCH METHODOLOGY

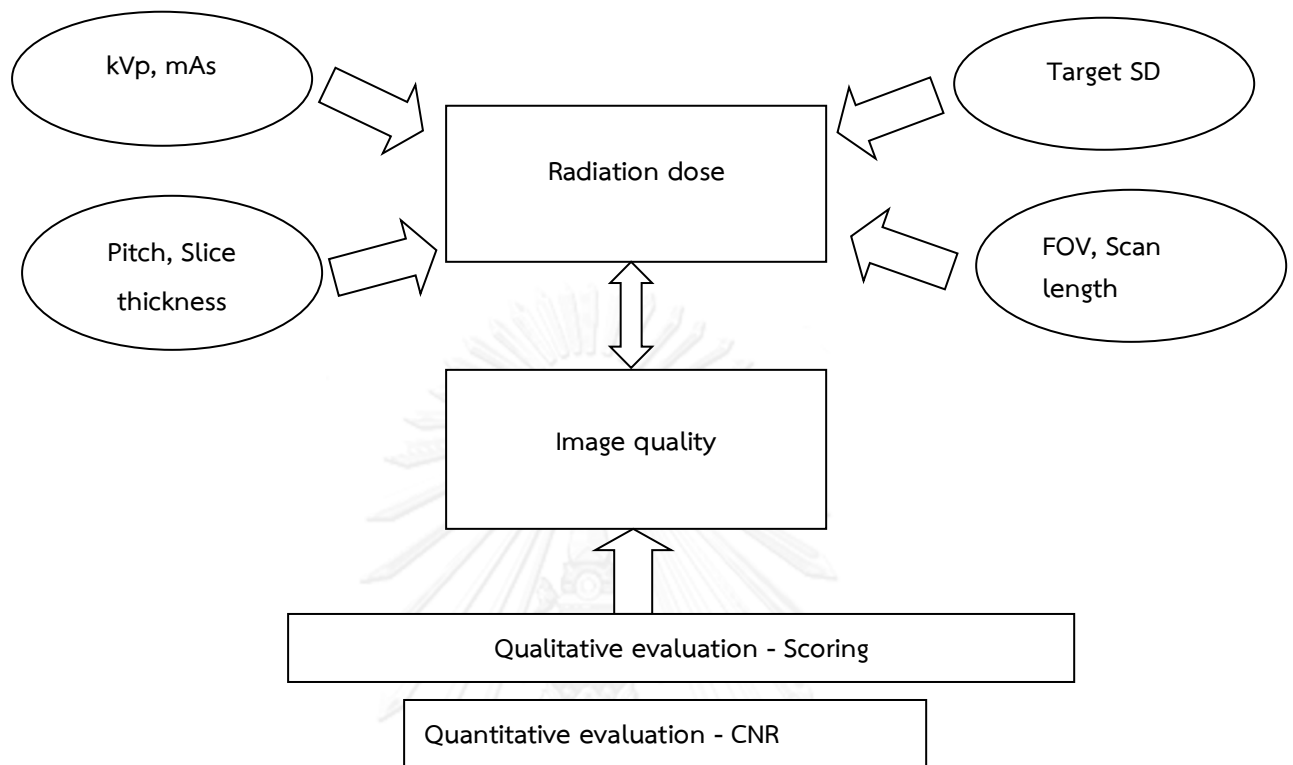
#### 3.1 Research design

This thesis is designed as an experimental prospective study.

#### 3.2 Research design model



### 3.3 Conceptual framework



### 3.4 Research question

What are the appropriate Target SD for radiation dose reduction at various beam pitch in 320-MDCT with optimal image quality in lung man phantom with nodules?

### 3.5 Materials

#### 3.5.1 CT scanner, Toshiba Aquilion ONE



Figure 3. 1 320 detector row CT Toshiba Aquilion ONE scanner

The CT scanner model Aquilion One, which range of kVp is 80 – 135 , range of mA is 10-580 , maximum coverage is 16 cm per rotation, 70 kW generator, 7.5 MHU x-ray tube and fastest gantry rotation time of 0.35 seconds manufactured by Toshiba as shown in Figure 3.1 was used to acquire CT images. The system was installed at the Department of Radiology, King Chulalongkorn Memorial Hospital in 2011.

#### 3.5.2 Lung man chest phantom study

Lung man chest phantom (Kyoto Kagaku Co.Ltd.) is designed and constructed commercially to simulate standard human chest. The inner components consist of mediastinum, pulmonary vasculature, abdomen block and synthetic bones as illustrated in Figure 3.2 have x-ray absorption rates relatively to those of human tissues. The standard size of the phantom equal 17 cm chest thickness as the man at 90 kg weight.



Figure 3. 2 Lung man chest phantom

### 3.5.3 Simulated lung nodules

Simulated lung nodules were attached in lung field of Lung man chest phantom. There are five sizes of simulated nodules which consist of nodule sphere of 12, 10, 8, 5 and 3 mm in diameters. The CT number of each nodule equal 100 Hounsfield Unit as shown in Figure 3.3.



Figure 3. 3 Simulated lung nodule of sphere 12, 10, 8, 5 and 3 mm in diameters

### 3.5.4 Catphan<sup>®</sup> 600 phantom

The CATPHAN phantom will be used to assess the image quality of CT system as shown in Figure 3.4 According to the design of the phantom, all test sections can be located by precisely indexing the table from center of section 1 (CTP404) to the center of each subsequent test module. The indexing distances from first section are listed as follows:

Module	Distance from section 1 center
CTP404, slice width, sensitometry and pixel size	
CTP591, Bead geometry	32.5 mm
CTP528, 21 line pair high resolution	70 mm
CTP528, Point source	80 mm
CTP515, Subslice and supra-slice low contrast	110 mm
CTP486, Solid image uniformity module	150 mm

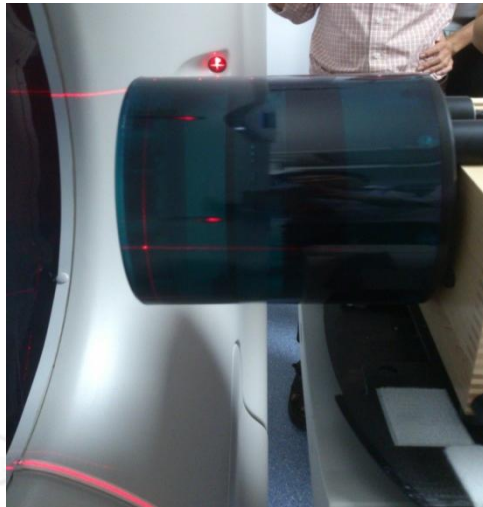


Figure 3. 4 Catphan<sup>®</sup> 600 Phantom

### 3.5.5 PMMA phantom

The PMMA phantom will be used to perform QC for CT system. The cylindrical phantoms consist of 16 cm in diameter for head phantom and 32 cm in diameter for body phantom. The phantom made of solid Polymethyl Methacrylate (PMMA) disks as shown in Figure 3.5 The phantom is designed with a center hole and eight peripheral holes for pencil ion chamber placement.

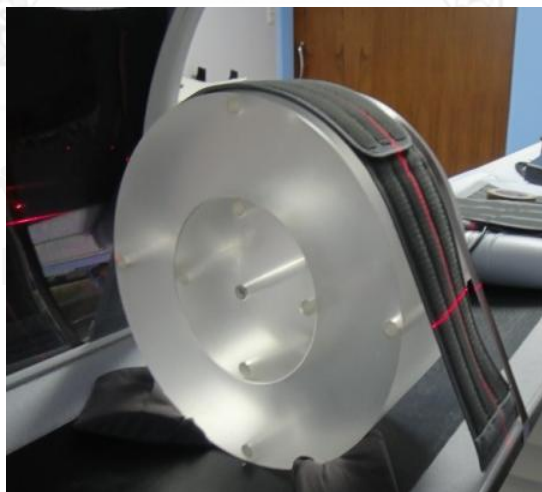


Figure 3. 5 Cylindrical PMMA phantom of 16 and 32 cm diameters

### 3.5.6 Unfors model Xi base unit with mAs display

The Unfors Xi as illustrated in Figure 3.6 is a complete system for multi-parameter measurements on all modalities. The detector is a solid state type which is not affected by the temperature and pressure of the environment.



Figure 3. 6 Unfors Raysafe model Xi base unit with mAs display

### 3.5.7 CT pencil-type ionization chamber

CT pencil-type ionization chamber of  $4.9 \text{ cm}^3$  active volume, 10 cm total active length is shown in Figure 3.7. The ion chamber and electronics are integrated into one unit making it available to measure both temperature and pressure to actively compensate for this dependency.



Figure 3. 7 10 cm length of the pencil-type ionization Unfors Xi CT Detector

### 3.6 Methods

#### 3.6.1 Perform the quality control of Toshiba Aquilion ONE

The quality control of Toshiba Aquilion ONE will be performed following the IAEA Human Health No.19. The quality control program consists of Mechanical accuracy, Dosimetry CTDI in air, CTDI in phantom and image performance.

#### 3.6.2 Verification of $C_{a,100}$

The  $C_{a,100}$  will be verified of all x-ray beam collimations for the accuracy, reproducibility and confidence of using these values. The procedures are as followings:

- The pencil ionization chamber will be placed on overhangs at the end of the scanner couch. The position of pencil ionization chamber will be ensuring to avoid the alignment errors.
- Computed Tomography Dose Index in air will be measured and recorded from dosimeter reading.
- The acquisition parameters will be 1 second rotation time, effective mAs 100 in axial mode by vary kVp and collimations.
- $C_{a,100}$  will be calculated for each kVp and collimations.

#### 3.6.3 Verification of $C_{VOL}$

The  $C_{VOL}$  displayed on the monitor of the console of CT scanner will be verified for the accuracy, reproducibility and confidence of using these values. The procedures are as followings:

- The pencil ionization chamber will be inserted in the 16 and 32 cm diameters of PMMA phantom. The positioning of the phantom and chamber will be determined to avoid the alignment errors.
- Computed Tomography Dose Index (CTDI) displayed on the CT monitor console and on Ray Safe dosimeter will be recorded when the chamber is inserted at the center and the peripheral positions in phantom and scanned three times for each kVp setting.
- The acquisition parameters are 4 x 4.0 mm collimation, 1 sec rotation time and effective mAs 100.
- The data shown on dosimeter will be calculated for  $C_{VOL}$  and compared to the displayed values on CT monitor console and IEC values for each kVp.



### 3.6.4 Image quality in Catphan phantom

The Catphan<sup>®</sup> 600 Phantom will be mounted on the phantom holder and placed at the center of CT gantry. The CTP515 module (Subslice and supra-slice low contrast) will be scanned for study the contrast to noise ratio, the CTP528 module (21 line pair resolution) will be used to study the high contrast resolution

#### 3.6.4.1 High contrast resolution

CTP528 module containing the high resolution test objects will be scanned by using the head technique with slice thickness 1 mm and standard filter. A single axial scan with setting parameter of 120 kVp, 300 mA, 1 sec rotation time, FOV 240 mm will be performed. Choose range of high contrast resolution test objects and magnify as necessary. An appropriate window width and level for the best visualization of the test objects will be select. The smallest test object visualized on the monitor will also record.

#### 3.6.4.2 Contrast to noise ratio

Scan the CTP515 module containing Subslice and supra-slice low contrast using the parameters the same as the high contrast resolution with slice thickness 5 mm and standard filter. An appropriate window and level for the best visualization of the test objects will be select. The CNR will be obtained by subtracting the mean CT number measured in the circular ROI of 15 mm diameter of object from the mean CT number measured phantom background at same ROI area, then divide by the standard deviation of the pixel values of the phantom background as in equation 3.1

$$\text{CNR} = (\text{CT}_c - \text{CT}_b) / \text{SD}_b \quad (3.1)$$

Where  $\text{CT}_c$  is the CT number in circular ROI of 15 mm-diameter,  $\text{CT}_b$  is the CT number of background and  $\text{SD}_b$  is a standard deviation of background.

The region of interest area is  $90 \text{ mm}^2$  placed at the supra slice Nominal target contrast level 0.5% and background [19] as illustrated in Figure 3.8

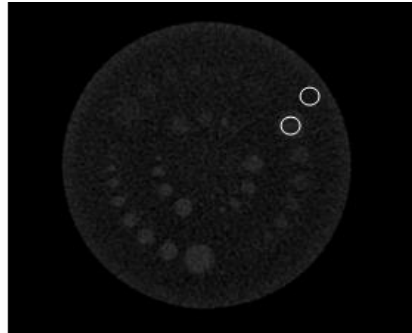


Figure 3. 8 Measurement the CT number of low contrast object and background

### 3.6.5 Phantom study

Lung man chest phantom will be scanned with variable parameters such as Target SD, pitch and kVp with standard filter. The five sizes of simulated nodule will be attached in the lung field of lung man phantom. The location of simulated nodules will be set by the followings as illustrated in Figure 3.9 :

3 mm 2/3 in peripheral of right middle lobe (red color)

5 mm 1/3 in peripheral of left upper lobe (blue color)

8 mm in right lower lobe (green color)

10 mm in peripheral of left lower lobe (pink color)

12 mm in right upper lobe (yellow color)

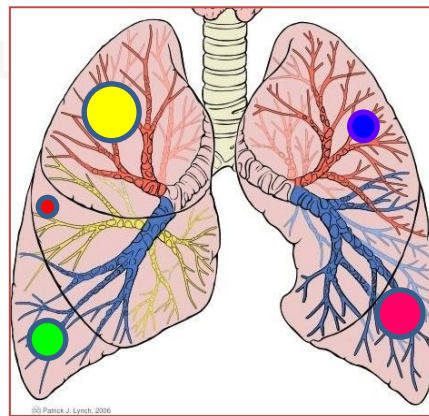


Figure 3. 9 The location of simulated nodules

The exposure technique for scan the phantom will be set by following the parameters:

kVp	120
Collimation (mm)	80 x 0.5
Pitch	0.813
Convolution filter	Standard filter
Slice thickness (mm)	1
Min mA – Max mA	10-400
Rotation time (s)	0.5
FOV (mm)	314
Scan length (mm)	360
Location	Apex of lung to lower costal margin

- The  $C_{VOL}$ , and DLP will be recorded from the CT monitor console.
- The Image quality will be determined in three majors characteristics consists of the nodule detection capability, contrast to noise ratio (CNR) and spatial resolution.

#### a) Contrast to noise ratio

The contrast to noise ratio (CNR) will be measured by placing the 2 circular ROIs of similar area within the nodule and background at the same slice as shown in Figure 3.9 with WW -600, WL 1600. The CT number within the ROI will be recorded to calculate the (CNR).

The CNR was define as in equation 3.2

$$CNR = (CT_n - CT_b) / SD_b \quad 3.2$$

Where  $CT_n$  is the CT number of nodule,  $CT_b$  is the CT number of background and  $SD_b$  is standard deviation of background.

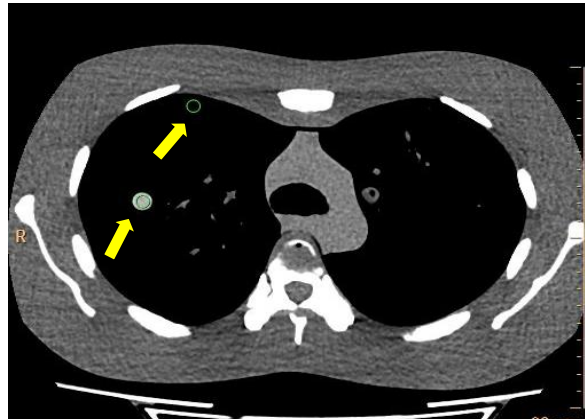


Figure 3. 10 Measurement the CT number of nodule and background

The CNR will be compared to those within the group of same kVp but varying Target SD and pitch in order to determine percent CNR. The CNR of different parameters in the group will be normalized at Target SD 9, pitch 0.813 and 120 kVp. The percent of CNR is defined as in equation 3.3

$$\%CNR = (CNR \times 100) / CNR_{(Target\ SD\ 9, Pitch\ 0.813, 120\ kVp)} \quad 3.3$$

#### The nodule detection capability

The nodule detection capability will be scored by two radiologists with similar experience. They are blinded trial to the scanning parameter techniques. The images will be displayed in the random order for each observer. The observers independently scored the image for nodule detection capability using a five point scale: score 1 means unsatisfactory; score 2 poor; score 3 acceptable; score 4 good and score 5 excellent.

#### b) Spatial resolution

Lung man chest phantom images will be reviewed. The spatial resolution will be assessed by the best visualize of the smallest size of simulated nodule using five point scale: score 5 = 3 mm visualized, score 4 = 5 mm visualized, score 3 = 8 mm visualized, score 2 = 10 mm visualized, score 1= 12 mm visualized with various parameters.

#### 3.6.6 Optimization of the radiation dose and image quality

The correlation of the radiation dose and image quality will be determined using lung man phantom to obtain to optimal protocols for CT chest with the appropriate Target SD according to the pitch and kVp by consider the lowest  $C_{VOL}$  with acceptable image quality

### 3.7 Data analysis

The quantitative image quality will be determined from the CNR and the spatial resolution (smallest nodule detected). The CNR will be evaluated by using Microsoft excel software to determine the mean, minimum and maximum values.

The qualitative image quality will be determined by two radiologists who have similar experience in CT. The five points scale will be used to assess the nodule detection capability as shown in Table 3.1 the agreement of image quality scored will be evaluated by calculating the weighted kappa of the variation of Target SD, pitch and kVp of the lung man chest phantom.

Table 3. 1 The five point scale for image quality

Score	Image quality	Criteria
1	Unsatisfactory	Visualize blur of all simulated nodules
2	Poor	Visualize 12 mm in diameter of simulated nodule or partly visualize 10 mm in diameter of simulated nodules
3	Acceptable	Visualize 8 and 10 mm in diameter of simulated nodule with sharp edge or partly visualize 5 mm in diameter of simulated nodule
4	Good	Visualize 5 mm in diameter of simulated nodule with sharp edge or partly visualize 3 mm in diameter of simulated nodule

Table 3.1 The five point scale for image quality

Score	Image quality	Criteria
5	Excellent	Visualize all simulated nodules with sharp edge

### 3.8 Sample size determination

This is an experimental (in vitro) study. The variable parameters were set. The sizes between two related groups are;

- Four values of Target SD
- Three values of beam pitch
- Two values of kVp

### 3.9 Statistical analysis

3.9.1 Descriptive statistics as mean, minimum and maximum by using Microsoft excel program

3.9.2 Weighted kappa for inter observer reliability will be used to evaluate qualitative image analysis from [www.medcalc.org/manual/kappa.php](http://www.medcalc.org/manual/kappa.php).

### 3.10 Outcome measurement

Variable: Independent variables = Target SD, Pitch, kVp

Dependent variables = %CNR, Nodule detection capability,  
Radiation Dose

### 3.11 Ethical consideration

This study is performed in phantom to determine the radiation dose and image quality of chest CT protocol. The research proposal has been approved by Ethical Committee of Faculty of Medicine, Chulalongkorn University

### 3.12 Expected benefit

3.12.1. Obtain appropriate target SD of image noise and beam pitch for lowest possible radiation dose with optimal image quality.

3.12.2. The optimal protocols benefit to reduce scan time and radiation dose to patient with increasing confidence in lung nodule-chest MDCT detectability.

3.12.3. Improve protocol for the clinical CT chest studies.



## CHAPTER IV

### RESULTS

#### 4.1 Quality control of the CT scanner: TOSHIBA Aquilion ONE

The quality control of CT scanner was performed following IAEA Human Health Series N0.19 [20] and IEC CT individual standard ( IEC 60601-2-44 Ed.2.1:2002). It includes the test of electromechanical component, image performance and radiation dose. The detail of quality control of results CT scanner is shown in Table 4.1 and Appendix B with the summarized report of CT scanner performance test.

Table 4. 1 Report of CT system performance

Location: CT unit, Chulachackapong Building, Floor.G

Date: 17 January 2013

Manufacturer: TOSHIBA

Model: AQUILION ONE

Pass Scan Localization Light Accuracy

Pass Alignment of Table to Gantry

Pass Table Increment Accuracy

Pass Slice Increment Accuracy

Pass Gantry Angle Tilt

Pass Reproducibility of CT Numbers

Pass mAs Linearity

Pass Linearity of CT Numbers

Pass Accuracy of Distance Measurement

Pass High Contrast Resolution

Pass Low Contrast Detectability

Pass Slice thickness accuracy

Pass Image uniformity



## 4.2 Verification of Computed Tomography Dose Index (CTDI)

### 4.2.1 Measurement CT air kerma index ( $C_{a,100}$ )

$C_{a,100}$  was measured using 100 mm pencil ion chamber set at the isocenter of the CT bore. The scan parameters were 100 mA tube current, 1 sec scan time and small focal spot size setting for all measurements at tube potential setting of 80, 100, 120 and 135. The results of  $C_{a,100}$  measurement are shown as in Table 4.2 and Table 4.3

Table 4. 2 The measured  $C_{a,100}$  in air for head protocols for each kVp and slice collimations.

kVp	$C_{a,100}$ (mGy) in air in Head protocol							
	Slice Collimation in mm (NT)							
	1(1x1)	2(0.5x4)	4 (1x4)	8(2x4)	12 (3x4)	16 (4x4)	20 (5x4)	32(8x4)
80	5.564	3.496	2.342	1.763	1.569	1.468	1.415	1.320
100	9.246	5.740	3.825	2.869	2.555	2.401	2.303	2.145
120	13.930	8.530	5.665	4.224	3.736	3.496	3.355	3.104
135	18.600	11.330	7.393	5.438	4.768	4.456	4.256	3.922

$C_{a,100}$  in air using head techniques 100 mAs, 240 mm FOV all Slice Collimations are plotted in Figure 4.1

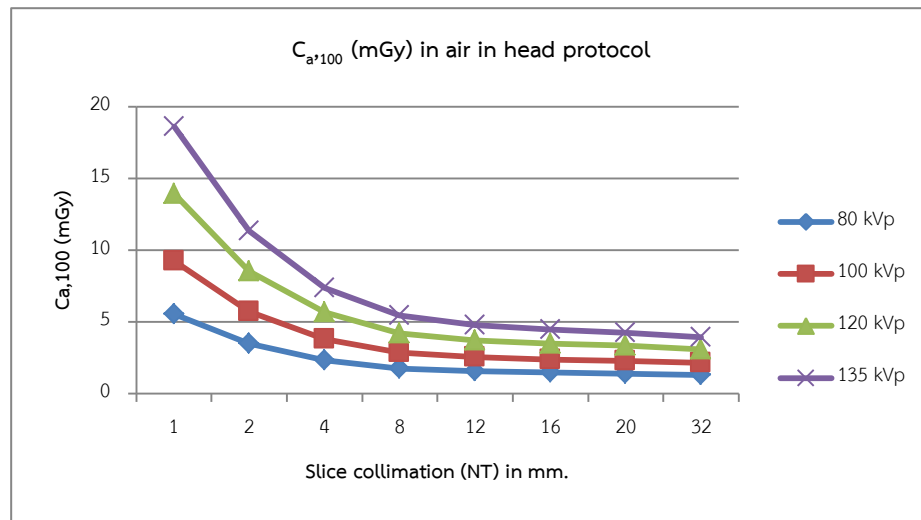


Figure 4. 1  $C_{a,100}$  in air, head protocol as the function of kVp and slice collimation are plotted in blue, red, green and violet colors at kVp of 80, 100, 120 and 135 respectively.

Table 4. 3 The measured  $C_{a,100}$  in air for body protocol for each kVp and slice collimation.

kVp	$C_{a,100}$ (mGy) in air in body protocol							
	Slice Collimation in mm (NT)							
	1(1x1)	2(0.5x4)	4 (1x4)	8(2x4)	12 (3x4)	16 (4x4)	20 (5x4)	32 (8x4)
80	6.066	3.526	2.258	1.600	1.357	1.254	1.188	1.098
100	7.711	4.761	3.195	2.406	2.137	1.997	1.923	1.782
120	12.100	7.380	4.885	3.634	3.218	3.009	2.888	2.672
135	16.570	9.990	6.508	4.798	4.193	3.904	3.733	3.441

$C_{a,100}$  in air using body techniques 100 mAs, 400 mm FOV all Slice Collimation are plotted in Figure 4.2

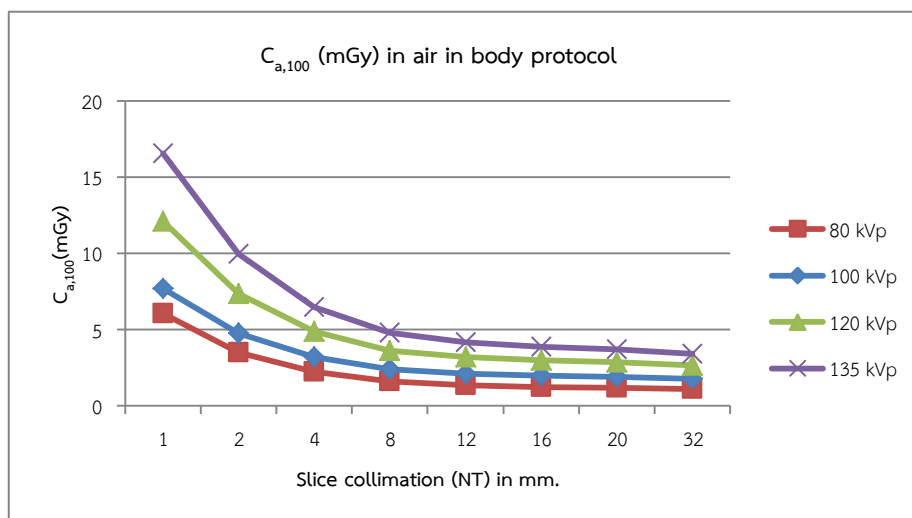


Figure 4. 2  $C_{a,100}$  in air, body protocol as the function of kVp and slice collimation are plotted in blue, red, green and violet colors of kVp 80, 100, 120 and 135 respectively.

#### 4.2.2 $C_{PMMA,100}$ in head phantom

The  $C_{PMMA,100}$  in head phantom was determined by using a 100 mm pencil ionization chamber placed in 5 holes of 16 cm diameter PMMA phantom at the isocenter of the CT bore. The scan parameters were 100 mA, 1 sec scan time, 240mm FOV and 4x4 mm collimation setting for all measurements at kVp 80, 100, 120 and 135 respectively.

Table 4. 4 The measured  $C_{PMMA,100}$  at each position of head phantom for each kVp,  $C_w$  and  ${}_nC_w$  in unit of mGy/mAs.

kVp	$C_{PMMA,100}$ in head phantom (mGy)						$C_w$ (mGy@100mAs)	${}_nC_w$ (mGy/mAs)
	At center	At peripheral						
		North	East	South	West			
80	6.856	8.45	8.34	7.71	7.65	7.64	0.07	

Table 4.4 The measured  $C_{PMMA,100}$  at each position of head phantom for each kVp,  $C_w$  and  ${}_nC_w$  in unit of mGy/mAs.

kVp	$C_{PMMA,100}$ in head phantom (mGy)						
	At center	At peripheral				$C_w$ (mGy@100mAs)	${}_nC_w$ (mGy/mAs)
		North	East	South	West		
100	12.99	16.09	14.46	13.31	14.63	14.08	0.14
120	20.24	22.95	21.66	21.48	20.97	21.26	0.21
135	26.83	33.26	30.34	28.83	29.15	29.21	0.29

#### 4.2.3 $C_{PMMA, 100}$ in body phantom

The  $C_{PMMA, 100}$  in body phantom was determined by using a 100 mm pencil ionization chamber placed in each hole of 32 cm diameter PMMA phantom at the isocenter of the CT bore. The scan parameters were 100 mA, 1 sec scan time, 400 mm FOV and 4x4 mm collimation setting for all measurements at kVp 80, 100, 120 and 135 respectively.

Table 4. 5 The measured  $C_{PMMA,100}$  at each position of body phantom for each kVp,  $C_w$  and  ${}_nC_w$  in unit of mGy/mAs.

kVp	$C_{PMMA,100}$ in body phantom (mGy)						
	At center	At peripheral				$C_w$ (mGy@100mAs)	${}_nC_w$ (mGy/mAs)
		North	East	South	West		
80	1.667	4.104	5.114	3.429	3.958	3.32	0.03
100	3.408	7.594	7.4813	6.228	7.369	5.91	0.06
120	5.953	12.994	11.681	10.125	11.556	9.71	0.09
135	8.056	16.231	16.888	13.894	15.669	13.13	0.13

#### 4.2.4 $C_{VOL}$ on monitor and calculated $C_w$

The  $C_w$  results in Table 4.4 and 4.5 The  $C_{VOL}$  displayed on CT monitor were recorded and compared with the calculated values in percent difference as shown in Table 4.6 for  $C_{VOL}$  in head phantom and Table 4.7 for  $C_{VOL}$  in body phantom.

Table 4. 6  $C_{VOL}$  displayed on monitor and calculated  $C_w$  using head techniques 100 mAs and 240 mm FOV, slice collimation 4x4 mm

kVp	$C_{VOL}$ in head phantom(mGy)		
	Calculated	Displayed	% difference
80	7.64	8.0	-4.5
100	14.08	14.7	-4.22
120	21.26	22.6	-5.93
135	29.21	29.9	-2.31

$C_{VOL}$  displayed on the monitor and the calculated  $C_w$  using head techniques mAs 100, collimation 16 mm and 240 mm FOV are plotted in Figure 4.3

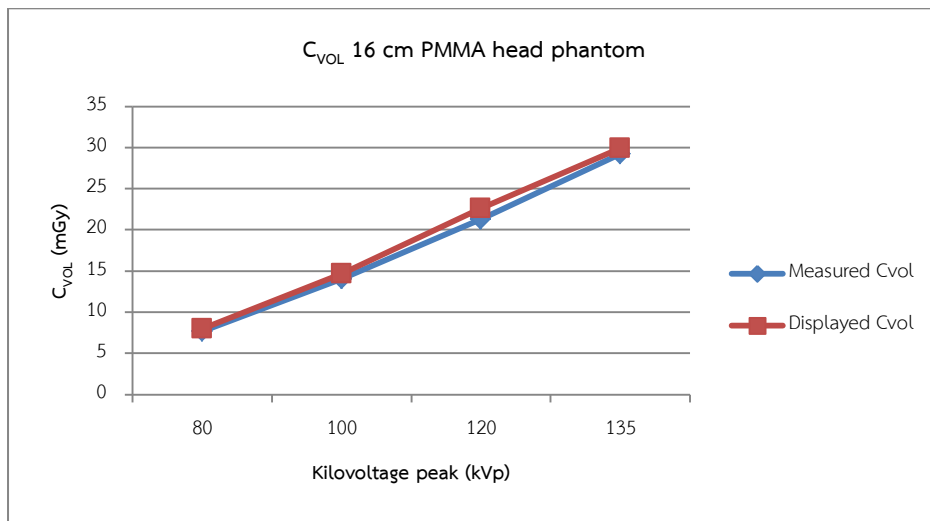


Figure 4. 3  $C_{VOL}$  (mGy) and  $C_w$  (mGy) of head phantom as the function of kVp are plotted in red (measured) and blue (displayed) straight lines of less than 10 percent discrepancy.

Table 4. 7  $C_{VOL}$  displayed on monitor and calculated  $C_w$  using body techniques 100 mAs and 400 mm FOV(L) slice collimation 4x4 mm

kVp	$C_{VOL}$ in body phantom(mGy)		% difference
	Calculated	Displayed	
80	3.32	3.4	-2.35
100	5.91	6.3	-6.19
120	9.71	10.4	-6.63
135	13.13	14.4	-8.82

$C_{VOL}$  displayed on the monitor and the calculated  $C_w$  using body techniques 100 mAs, collimation 16 mm and 400 mm FOV are plotted in Figure 4.4

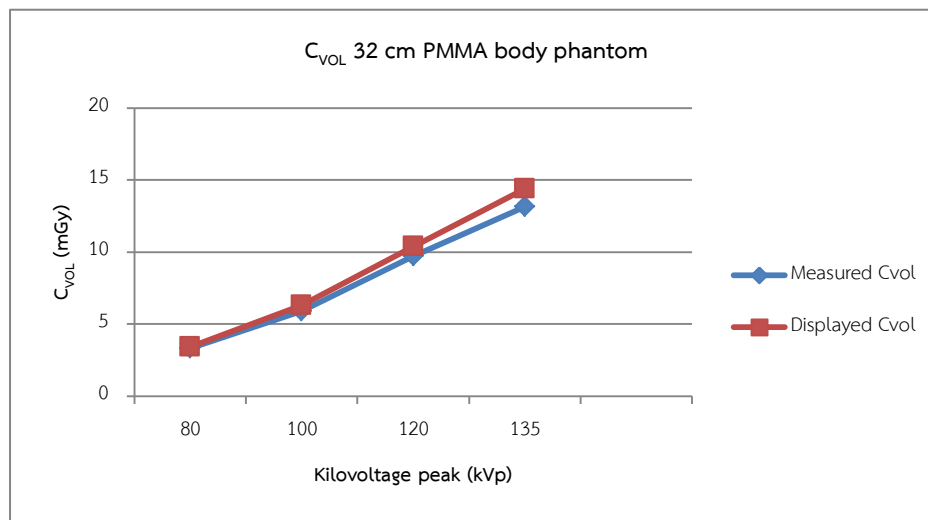


Figure 4. 4  $C_{VOL}$  (mGy) and  $C_w$  (mGy) of body phantom as the function of kVp are plotted red (measured) and blue (displayed) straight lines of less than 10 percent discrepancy.

#### 4.2.5 The measured $C_{VOL}$ of monitor and calculated $C_w$ compared with IEC values for 120 kVp

The results of  $C_{VOL}$  of monitor and  $C_w$  using head technique 100 mA, 1-s scan, Scan field: S (240 mm) 4 mm x 4 slice thickness compared with IEC are illustrated as in Table 4.8

Table 4. 8 The measured  $C_{VOL}$  of monitor and calculated  $C_w$  compared with IEC values using head technique 100 mA, 1-s, Scan field: S (240 mm) 4 mm x 4 slice thickness

$C_{VOL}$ (mGy) in head phantom						
kVp	$C_{VOL}$ (mGy)		%difference	IEC	%difference	%difference
	Calculated	Monitor	(monitor and calculated)		(Calculated and IEC)	(monitor and IEC)
120	21.26	22.60	-5.93	23.64	-10.07	-4.40

The results of  $C_{VOL}$  of monitor and  $C_w$  using Body technique 100 mA, 1-s scan Scan field: L (400 mm) 4 mm x 4 slice thickness compared with IEC are illustrated as in Table 4.9

Table 4. 9 The measured  $C_{VOL}$  of monitor and calculated  $C_w$  compared with IEC values using body technique 100 mA, 1-s, Scan field: L (400 mm) 4 mm x 4 slice thickness

kVp	$C_{VOL}$ (mGy) in Body phantom					
	Calculated	Monitor	%difference (monitor and calculated)	IEC	%difference (Calculated and IEC)	%difference (monitor and IEC)
120	9.71	10.4	-6.63	11.69	-16.94	-11.04

#### 4.3 Characteristic of image quality in Catphan phantom

The Catphan 600 phantom was used to study the image quality which contained two characteristics, Contrast to Noise Ratio (CNR) and spatial resolution. The CTP 515 was used to study CNR, while the CTP528 was used to study the spatial resolution.

##### 4.3.1 Contrast to Noise Ratio

The scanning parameter of head technique 120 kVp, 300 mA, 1 s rotation time, FOV 240 mm and slice thickness 1 mm were used with soft tissue window. The window and level (WW60, WL 360) were adjusted. The results of the CNR of the CTP 515 of Catphan phantom are illustrated as in Table 4.10

Table 4. 10 The measured of CT number (HU) of low contrast object and background values and calculate CNR of Catphan phantom

	CT number (HU)	SD
Low contrast object	48.68	-
Background	42.50	3.33
CNR	1.85	



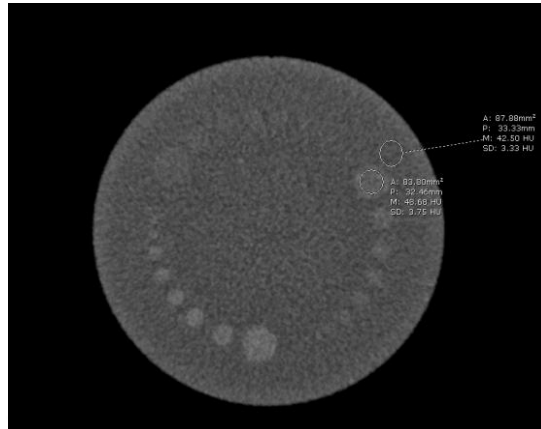


Figure 4. 5 Measurement the CT number of low contrast object and background

#### 4.3.2 Spatial resolution

The scanning parameter of head technique 120 kVp, 300 mA, 1 s rotation time, FOV 240 mm and slice thickness 1 mm were used with soft tissue window and lung window. Appropriate window and level were adjusted for the best visualization of the test objects. The results of lp/cm and gap size were shown in Table 4.11

Table 4. 11 Spatial resolution

Slice Thickness in mm	Resolution (lp/cm)
1 (soft tissue window)	7 (0.071mm)
1 (lung window)	7 (0.071mm)



Figure 4. 6 Spatial resolution part of Catphan phantom

#### 4.4 Radiation dose

$C_{VOL}$  and DLP were recorded from CT monitor console with scanning Lung man chest phantom with parameters 120 kVp collimation 80 x 0.5 mm pitch 0.813, standard filter, slice thickness 1 mm 10-400 min mA – max mA values, rotation time 0.5 s, FOV 314 mm, scan length 360 mm, location: apex of lung to lower costal margin and vary the Target SD, pitch and kVp. The data was shown in Table 4.12 and Table 4.13

Table 4. 12  $C_{VOL}$ , DLP of Lung man phantom at 120 kVp

kVp	Pitch	Target SD	$C_{VOL}$ (mGy)	DLP (mGy.cm)
120	0.637	9	7	252.0
120	0.637	14	3.1	111.6
120	0.637	20	1.2	43.2
120	0.637	25	0.9	32.4
120	0.813	9	5.9	212.4
120	0.813	14	3.5	126.0
120	0.813	20	1.1	39.6
120	0.813	25	0.7	25.2
120	1.388	9	6.5	234.0
120	1.388	14	2.7	97.2
120	1.388	20	1.3	46.8
120	1.388	25	0.9	32.4

Table 4. 13  $C_{VOL}$ , DLP of Lung man phantom at 100 kVp

kVp	Pitch	Target SD	$C_{VOL}$ (mGy)	DLP (mGy.cm)
100	0.637	9	6	216.0
100	0.637	14	2.4	86.4
100	0.637	20	1.3	46.8
100	0.637	25	0.8	28.8
100	0.813	9	5.3	190.8
100	0.813	14	2.5	90.0
100	0.813	20	1.2	43.2
100	0.813	25	0.8	28.8
100	1.388	9	6.2	223.2
100	1.388	14	2.4	82.8
100	1.388	20	1.4	50.4
100	1.388	25	0.9	32.4

The mean values  $C_{VOL}$  from pitch 0.637, 0.813, 1.388 of Lung man chest phantom were plotted when varying Target SD from 9 to 25 at 120 kVp as shown in Figure 4.7

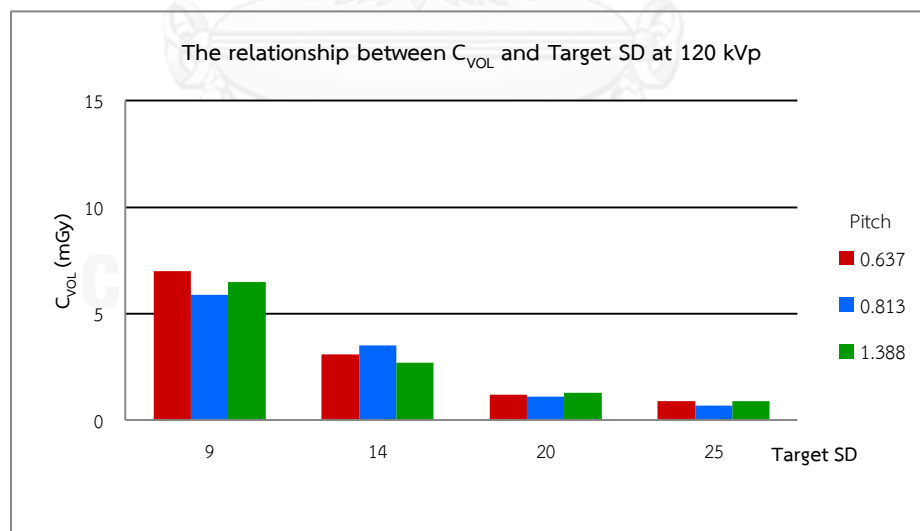
Figure 4. 7 The relationship between  $C_{VOL}$  and Target SD with different pitch at 120 kVp

Table 4. 14 The percent  $C_{VOL}$  reduction with increasing Target SD from 9 to 25 and increasing pitch at 120 kVp

Pitch	% $C_{VOL}$ reduction			
	Target SD			
	9	14	20	25
0.637	+18.64	47.54	79.66	84.74
0.813	0	40.68	81.35	88.14
1.388	+10.17	54.24	77.97	84.74

From Table 4.14 when increasing Target SD from 9 to 25, results in  $C_{VOL}$  reduction, at pitch 0.813 on Target SD 25 get the 88.14 %  $C_{VOL}$  reduction.

The mean values of  $C_{VOL}$  from pitch 0.637, 0.813, 1.388 of Lung man chest phantom were plotted when increasing Target SD from 9 to 25 at 100 kVp as shown in Figure 4.8

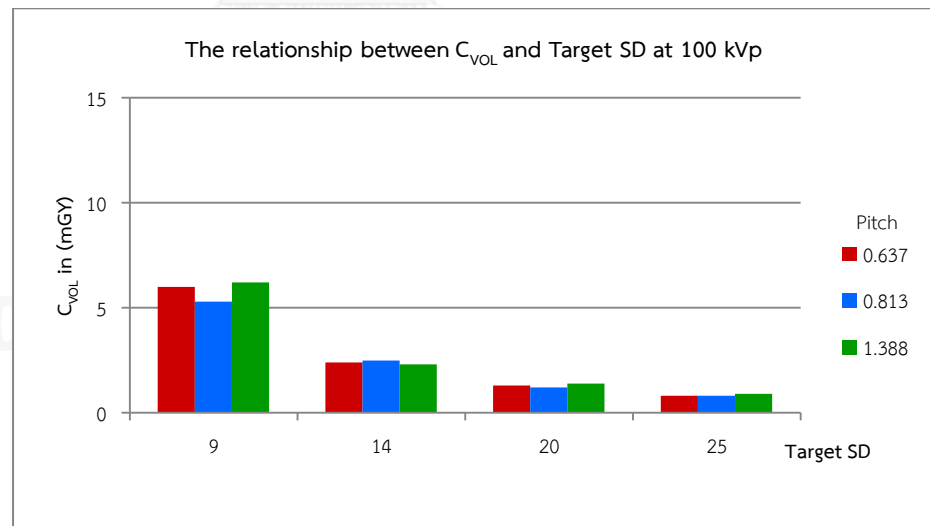


Figure 4. 8 The relationship between  $C_{VOL}$  and Target SD with different pitch at 100 kVp

Table 4. 15 The percent  $C_{VOL}$  reduction with increasing Target SD from 9 to 25 and increasing pitch at 100 kVp

Pitch	% $C_{VOL}$ reduction			
	Target SD			
	9	14	20	25
0.637	+1.69	59.32	77.97	86.44
0.813	10.16	57.63	79.66	86.44
1.388	+5.08	61.02	77.97	84.75

From Table 4.15 when increasing Target SD from 9 to 25, results in  $C_{VOL}$  reduction, at pitch 0.637, 0.813 on Target SD 25 get the 86.44 %  $C_{VOL}$  reduction.

The mean DLP from pitch 0.637, 0.813, 1.388 of Lung man chest phantom were plotted when varying Target SD from 9 to 25 at 120 and 100 kVp as shown in Figure 4.9 and Figure 4.10

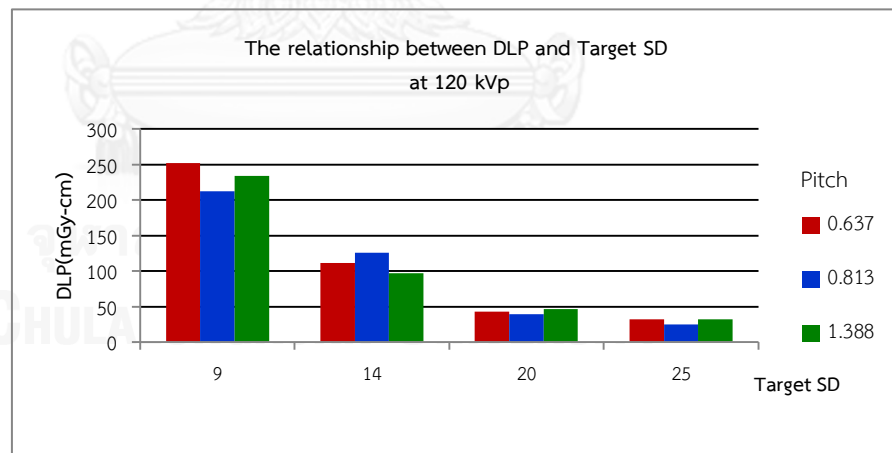


Figure 4. 9 The relationship between DLP and Target SD with different pitch at 120 kVp

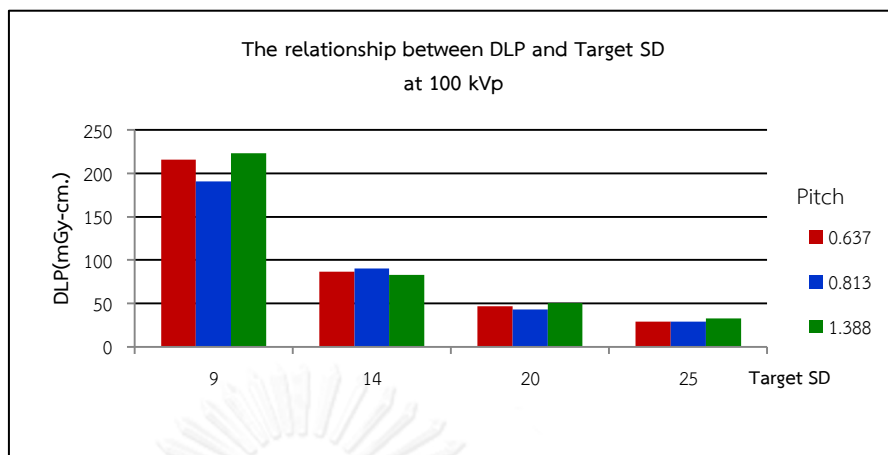


Figure 4. 10 The relationship between DLP and Target SD with different pitch at 100 kVp

## 4.5 Image quality

### 4.5.1 Quantitative image quality

#### 4.5.1.1 Contrast to Noise Ratio (CNR)

The percent CNR of standard size phantom was compared with the group of same both nodules and kVp with increasing pitch and Target SD. The CNR were normalized at Target SD 9, pitch 0.813 and 120 kVp as shown in Table 4.16 to 4.25

Table 4. 16 The percent CNR of nodule 12 mm in diameter for soft tissue window

kVp	Target SD	%CNR of nodule 12 mm		
		Pitch		
		0.637	0.813	1.388
120	9	102.17	100	82.91
	14	97.08	78.61	68.55
	20	66.22	55.74	55.91
	25	59.25	56.79	53.75
100	9	90.41	87.91	83.41
	14	81.98	79.75	74.16
	20	62.68	55.82	52.35
	25	54.37	50.59	50.14

Table 4.16 shows the decreasing percent CNR of nodule 12 mm diameter with increasing pitch and Target SD for soft tissue window.

Table 4. 17 The percent CNR of nodule 10 mm in diameter for soft tissue window

kVp	Target SD	%CNR of nodule 10 mm		
		Pitch		
		0.637	0.813	1.388
120	9	104.11	100	80.31
	14	90.76	75.72	70.56
	20	82.67	64.08	55.12
	25	58.44	56.42	50.91
100	9	93.52	85.4	81.17
	14	85.86	70.62	70.60
	20	64.06	58.23	55.84
	25	55.58	53.84	51.06

Table 4.17 shows the decreasing percent CNR of nodule 10 mm diameter with increasing pitch and Target SD for soft tissue window.



Table 4. 18 The percent CNR of nodule 8 mm in diameter for soft tissue window

kVp	Target SD	%CNR of nodule 8 mm		
		Pitch		
		0.637	0.813	1.388
120	9	102.52	100	95.75
	14	87.11	84.91	83.68
	20	61.71	59.82	58.28
	25	59.59	56.19	53.72
100	9	91.21	88.64	86.78
	14	85.12	79.94	65.36
	20	60.46	59.05	57.56
	25	55.95	54.34	52.37

Table 4.18 shows the decreasing percent CNR of nodule 8 mm diameter with increasing pitch and Target SD for soft tissue window.

Table 4. 19 The percent CNR of nodule 5 mm in diameter for soft tissue window

kVp	Target SD	%CNR of nodule 5 mm		
		Pitch		
		0.637	0.813	1.388
120	9	118.57	100	93.71
	14	82.64	82.85	79.10
	20	64.72	61.81	59.72
	25	60.26	54.59	55.23
100	9	91.51	89.13	83.79
	14	80.43	78.76	76.04
	20	59.65	57.12	56.55
	25	53.94	53.08	50.70

Table 4.19 shows the decreasing percent CNR of nodule 5 mm diameter with increasing pitch and Target SD for soft tissue window.

Table 4. 20 The percent CNR of nodule 3 mm in diameter for soft tissue window

kVp	Target SD	%CNR of nodule 3 mm		
		Pitch		
		0.637	0.813	1.388
120	9	102.65	100	90.57
	14	80.37	76.39	68.74
	20	58.62	56.42	55.16
	25	51.39	49.75	47.74
100	9	94.32	88.80	85.80
	14	79.52	73.32	70.02
	20	56.79	55.86	53.80
	25	48.75	44.04	45.85

Table 4.20 shows the decreasing percent CNR of nodule 3 mm diameter with increasing pitch and Target SD for soft tissue window.

Table 4. 21 The percent CNR of nodule 12 mm in diameter for lung window

kVp	Target SD	%CNR of nodule 12 mm		
		Pitch		
		0.637	0.813	1.388
120	9	105.66	100	81.78
	14	93.06	80.8	68.18
	20	67.76	54.95	58.59
	25	56.12	51.38	52.03
100	9	93.44	89.81	86.39
	14	82.24	81.45	76.95
	20	69.33	57.24	51.70
	25	57.62	53.58	52.34

Table 4.21 shows the decreasing percent CNR of nodule 12 mm diameter with increasing pitch and Target SD for lung window.

Table 4. 22 The percent CNR of nodule 10 mm in diameter for lung window

kVp	Target SD	%CNR of nodule 10 mm		
		Pitch		
		0.637	0.813	1.388
120	9	111.81	100	82.26
	14	95.80	77.96	71.22
	20	84.81	68.83	58.16
	25	59.69	56.4	53.65
100	9	101.81	98.64	90.22
	14	85.42	78.25	76.01
	20	61.74	63.49	55.80
	25	60.72	55.52	51.08

Table 4.22 shows the decreasing percent CNR of nodule 10 mm diameter with increasing pitch and Target SD for lung window.

Table 4. 23 The percent CNR of nodule 8 mm in diameter for lung window

kVp	Target SD	%CNR of nodule 8 mm		
		Pitch		
		0.637	0.813	1.388
120	9	110.98	100	98.00
	14	88.25	85.82	84.52
	20	63.70	60.88	58.52
	25	60.85	57.66	55.48
100	9	93.45	89.46	87.07
	14	86.8	81.37	66.13
	20	66.00	61.23	57.77
	25	61.14	55.63	54.08

Table 4.23 shows the decreasing percent CNR of nodule 8 mm diameter with increasing pitch and Target SD for lung window.

Table 4. 24 The percent CNR of nodule 5 mm in diameter for lung window

kVp	Target SD	%CNR of nodule 5 mm		
		Pitch		
		0.637	0.813	1.388
120	9	122.43	100	95.81
	14	103.52	93.53	81.53
	20	82.57	78.07	61.35
	25	66.72	59.81	57.72
100	9	109.95	97.66	90.04
	14	89.79	83.51	81.39
	20	73.71	69.62	63.39
	25	65.48	63.45	60.44

Table 4.24 shows the decreasing percent CNR of nodule 5 mm diameter with increasing pitch and Target SD for lung window

Table 4. 25 The percent CNR of nodule 3 mm in diameter for lung window

kVp	Target SD	%CNR of nodule 3 mm		
		Pitch		
		0.637	0.813	1.388
120	9	108.17	100	92.92
	14	87.10	78.44	70.77
	20	60.09	58.33	58.17
	25	52.68	50.97	49.63
100	9	106.40	90.32	86.75
	14	87.48	75.44	73.44
	20	58.37	56.52	57.98
	25	53.89	51.54	50.54

Table 4.25 shows the decreasing percent CNR of nodule 3 mm diameter with increasing pitch and Target SD for lung window

The percent CNR of soft tissue window and lung window were plotted for the relationship between the CNR and Target SD when increasing the pitch compare with the same size of nodule as shown in Figure 4.11-4.15 for soft tissue window at 120 and 100 kVp and Figure 4.16-4.20 for lung window at 100 and 120 kVp.



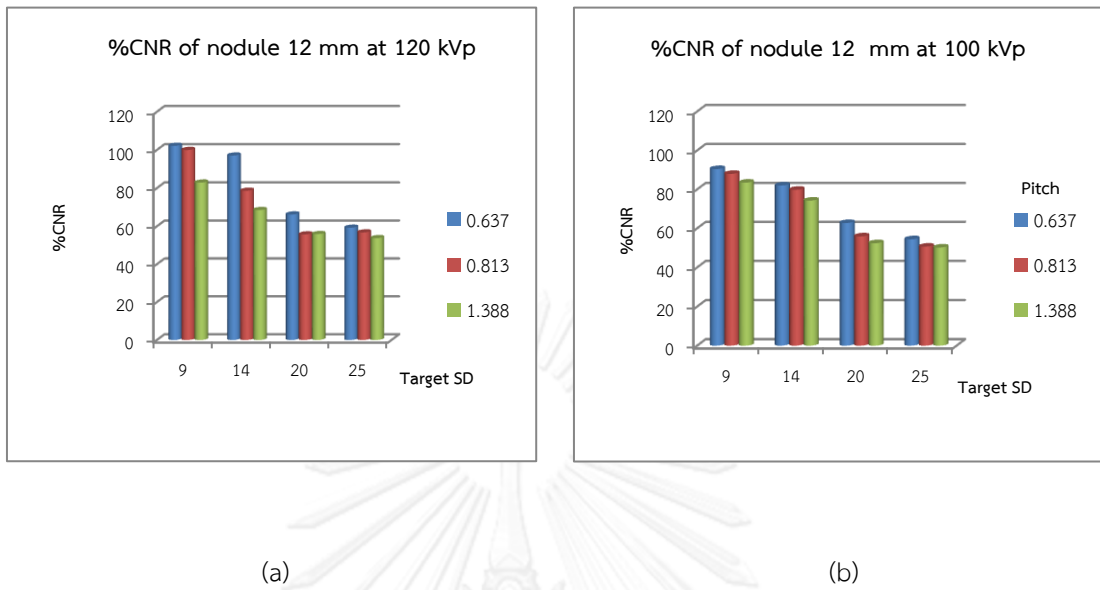


Figure 4. 11 The percent CNR of nodule 12 mm, at 120 (a) and 100 kVp (b) for soft tissue window

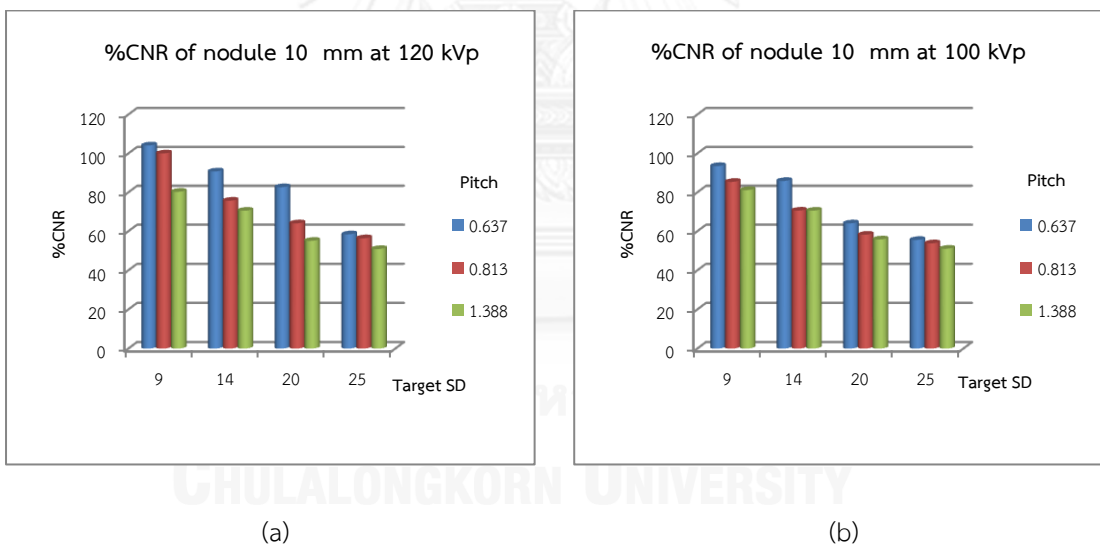
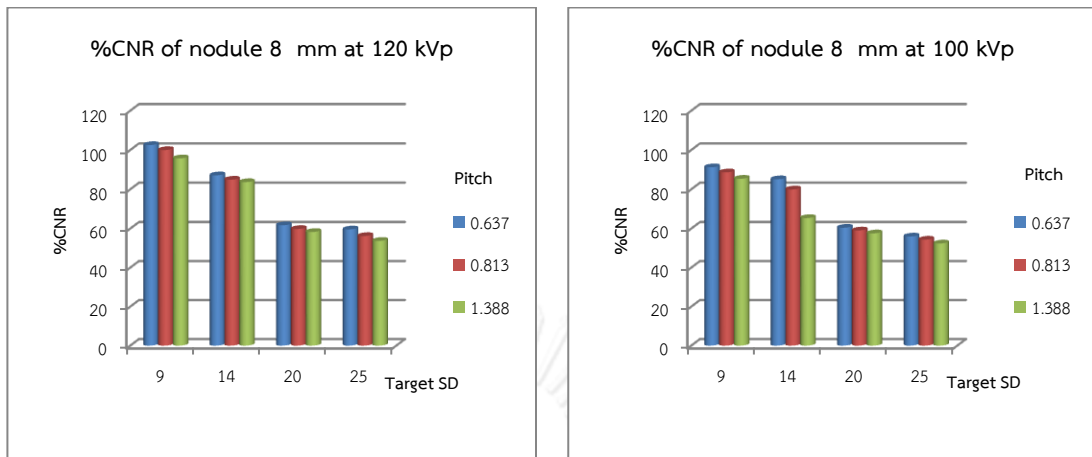


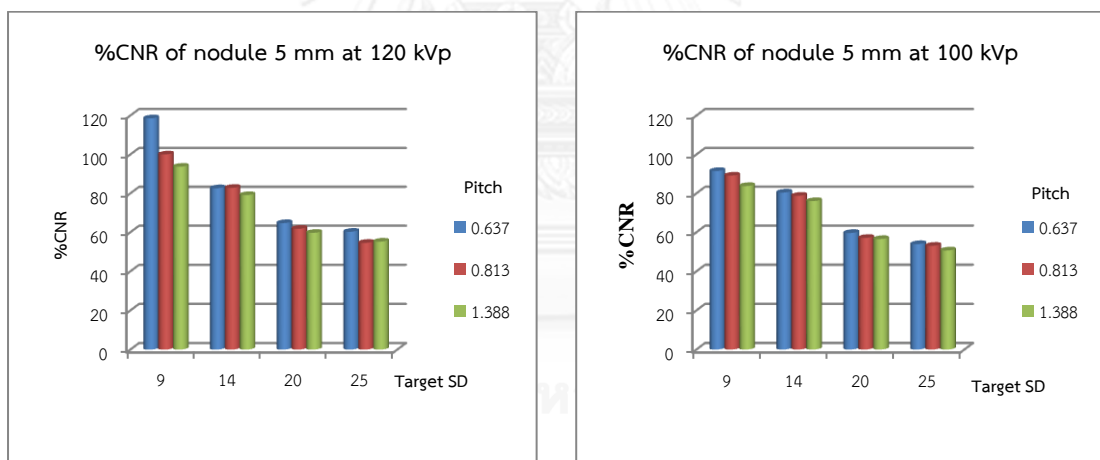
Figure 4. 12 The percent CNR of nodule 10 mm, at 120 (a) and 100 kVp (b) for soft tissue window



(a)

(b)

Figure 4. 13 The percent CNR of nodule 8 mm, at 120 (a) and 100 kVp (b) for soft tissue window



(a)

(b)

Figure 4. 14 The percent CNR of nodule 5 mm, at 120 (a) and 100 kVp (b) for soft tissue window

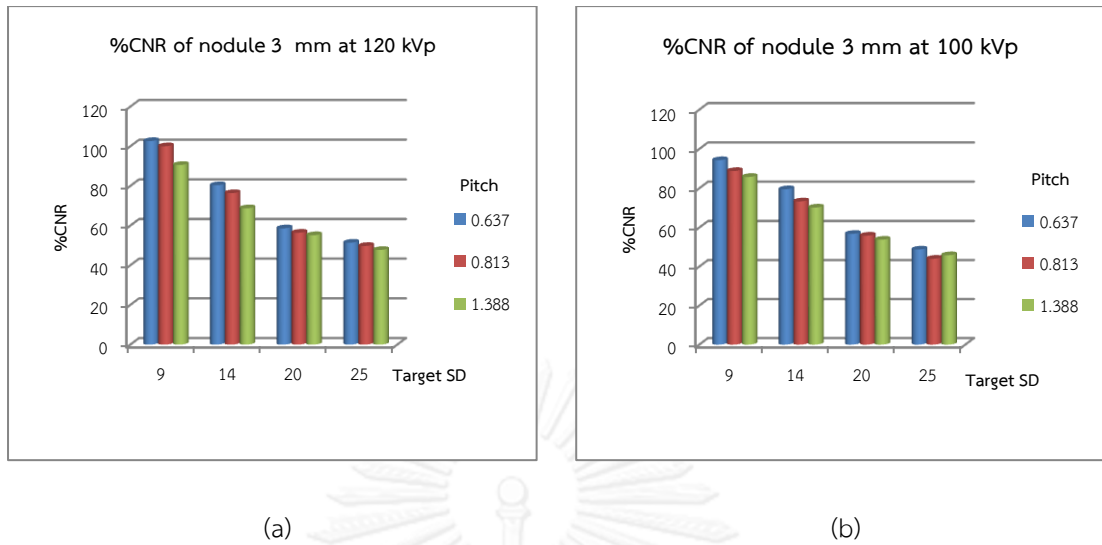


Figure 4. 15 The percent CNR of nodule 3 mm, at 120 (a) and 100 kVp (b) for soft tissue window

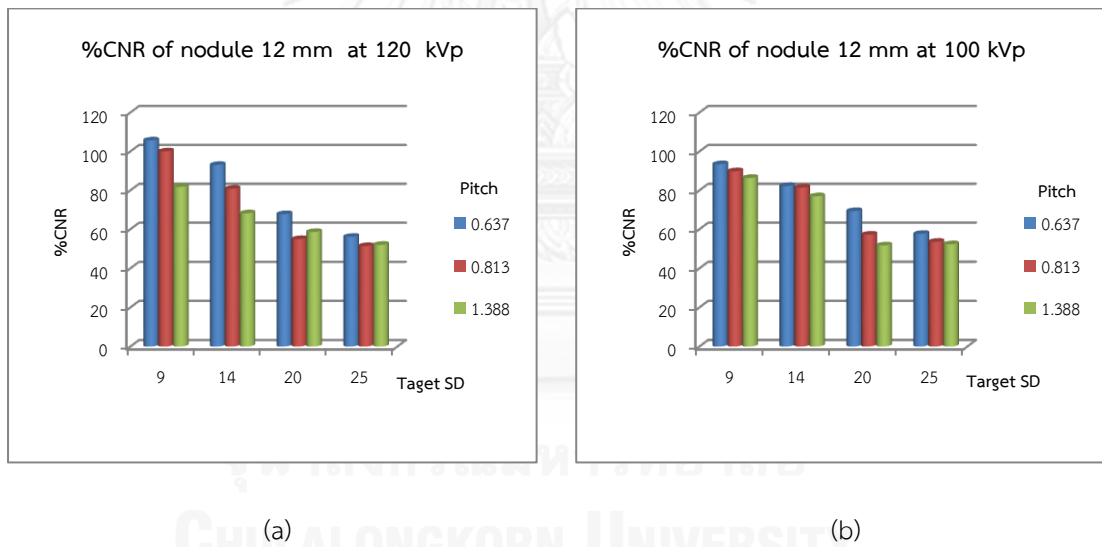
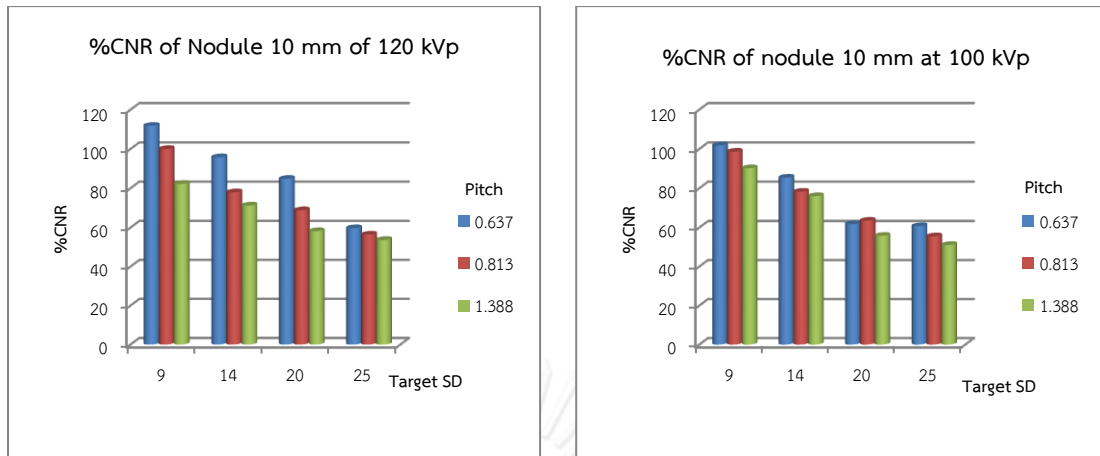


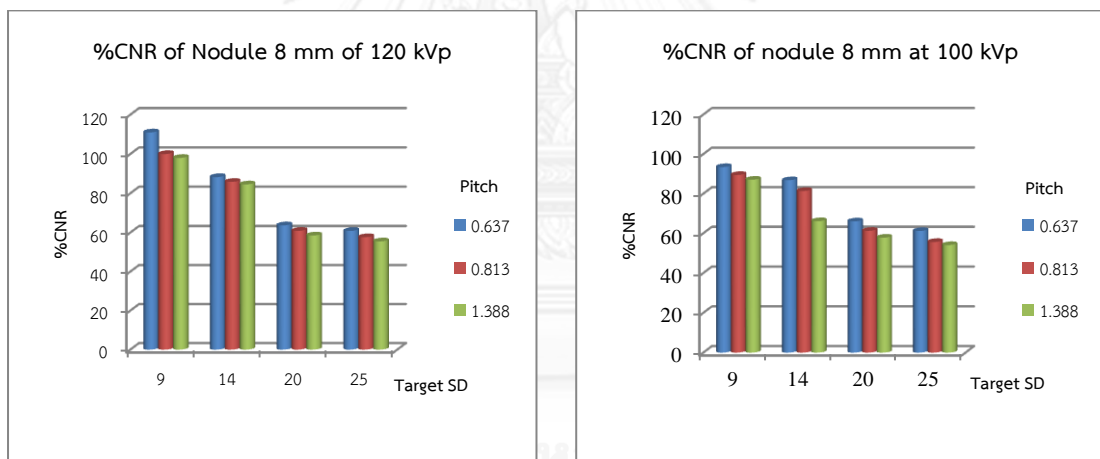
Figure 4. 16 The percent CNR of nodule 12 mm, at 120 (a) and 100 kVp (b) for lung window



(a)

(b)

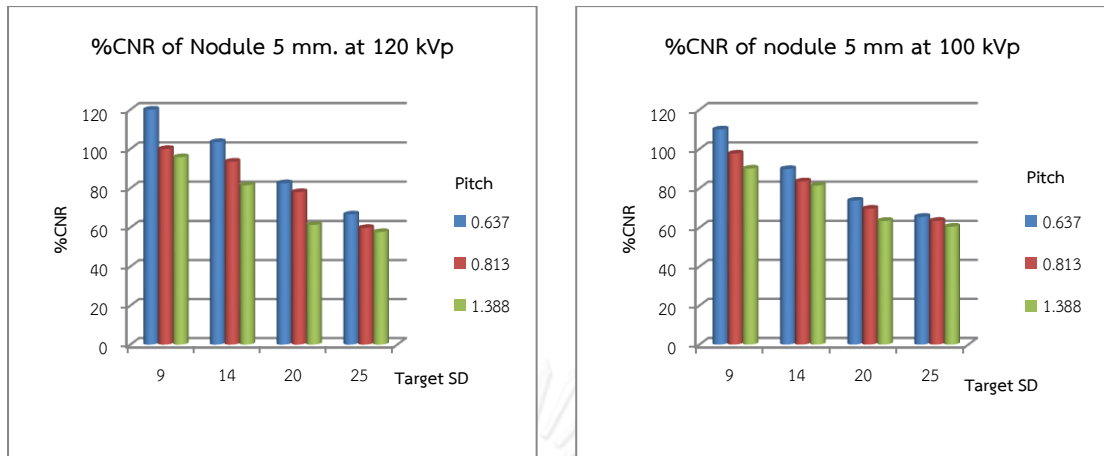
Figure 4. 17 The percent CNR of nodule 10 mm, at 120 (a) and 100 kVp (b) for lung window



(a)

(b)

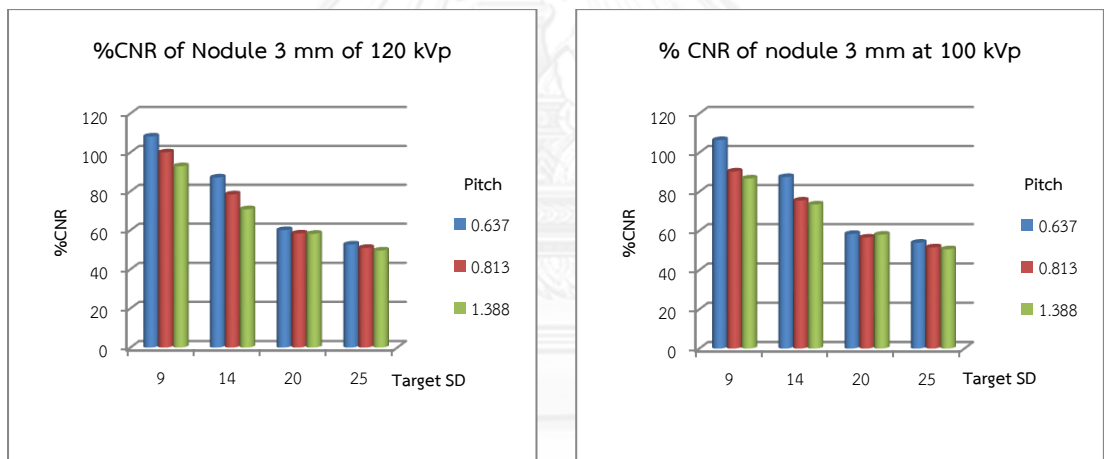
Figure 4. 18 The percent CNR of nodule 8 mm, at 120 (a) and 100 kVp (b) for lung window



(a)

(b)

Figure 4. 19 The percent CNR of nodule 5 mm, at 120 (a) and 100 kVp (b) for lung window

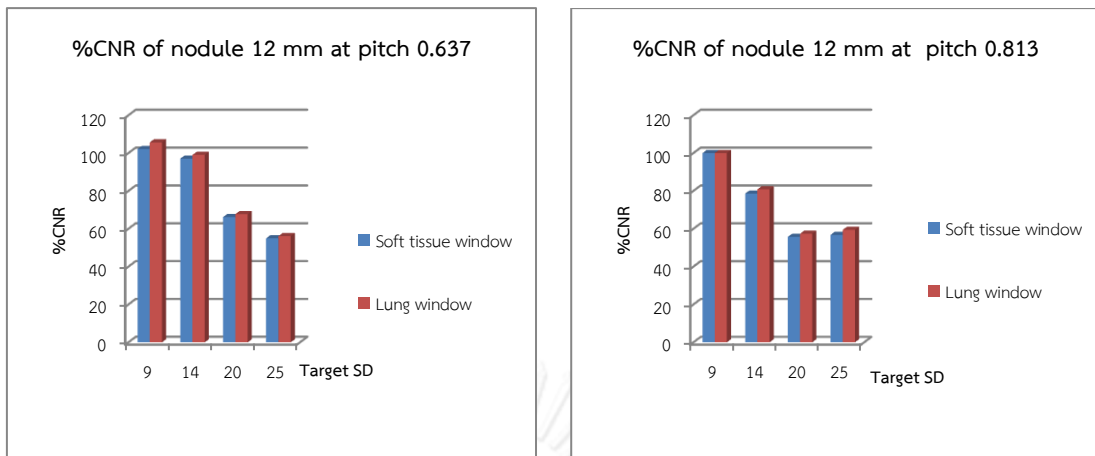


(a)

(b)

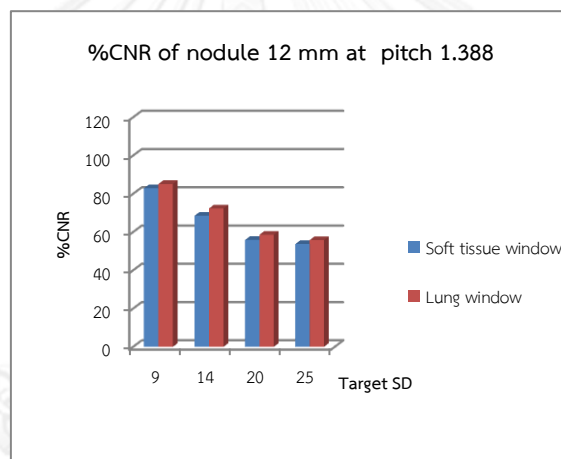
Figure 4. 20 The percent CNR of nodule 3 mm, at 120 (a) and 100 kVp (b) for lung window

The percent CNR of soft tissue window and lung window were plotted for the relationship between the CNR and Target SD when increasing the pitch then compare between soft tissue window and lung window with the same size of nodule as shown in Figure 4.21-4.25 for 120 kVp and Figure 4.26-4.30 for 100 kVp



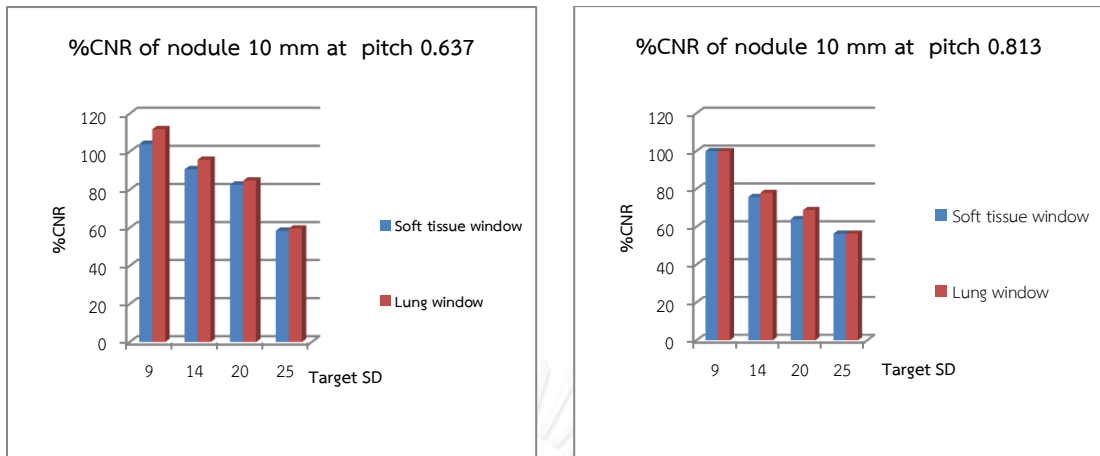
(a)

(b)



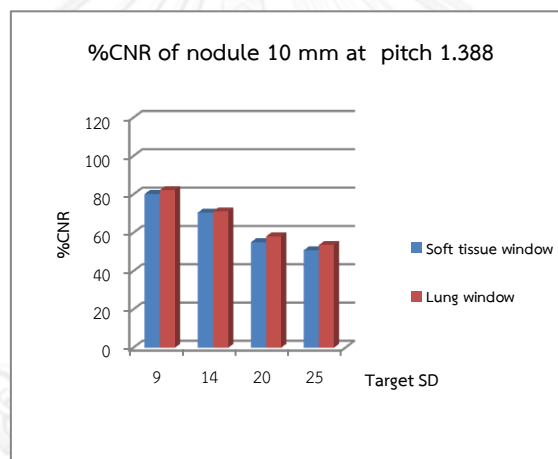
(c)

Figure 4. 21 The percent CNR of nodule 12 mm, at 120 kVp compared between soft tissue window and lung window for pitch 0.637 (a), pitch 0.813 (b) and pitch 1.388 (c)



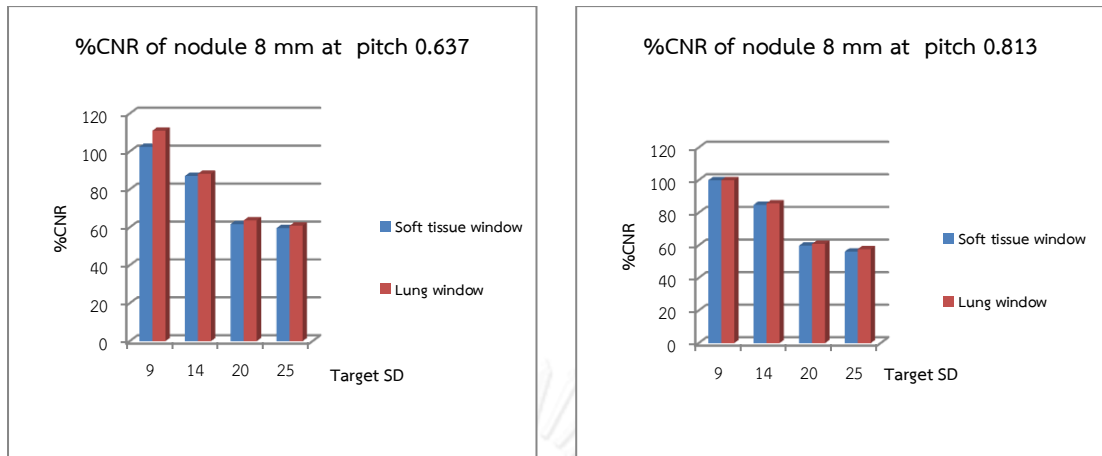
(a)

(b)



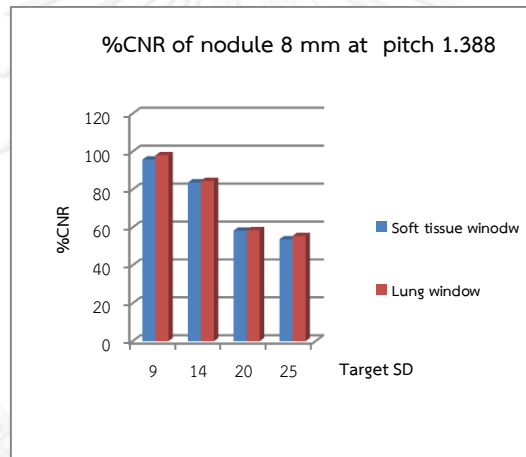
(c)

Figure 4. 22 The percent CNR of nodule 10 mm, at 120 kVp compared between soft tissue window and lung window for pitch 0.637 (a), pitch 0.813 (b) and pitch 1.388 (c)



(a)

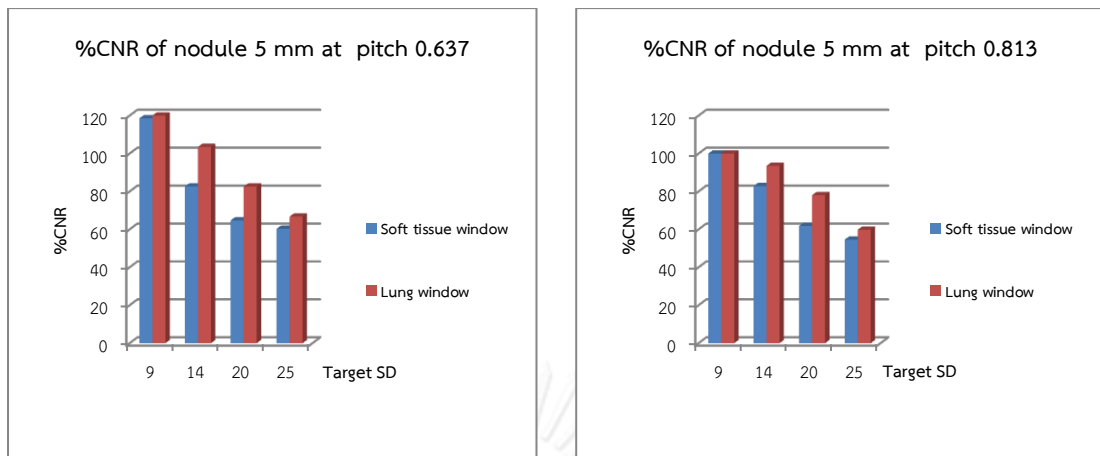
(b)



(c)

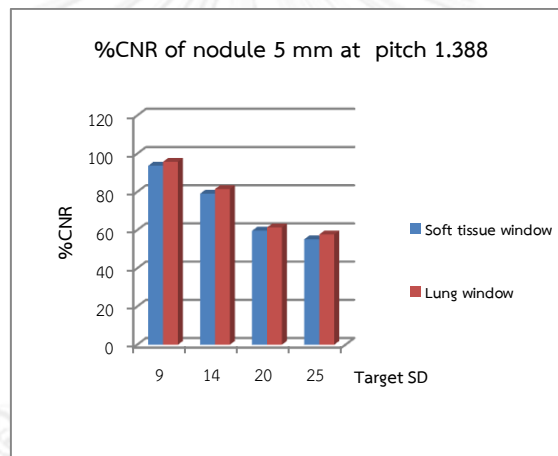
Figure 4. 23 The percent CNR of nodule 8 mm, at 120 kVp compared between soft tissue window and lung window for pitch 0.637 (a), pitch 0.813 (b) and pitch 1.388 (c)





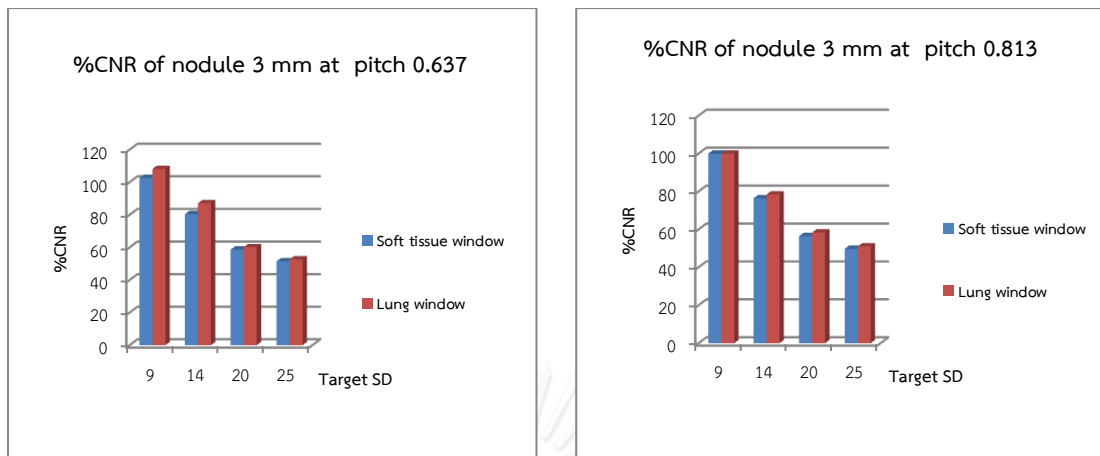
(a)

(b)



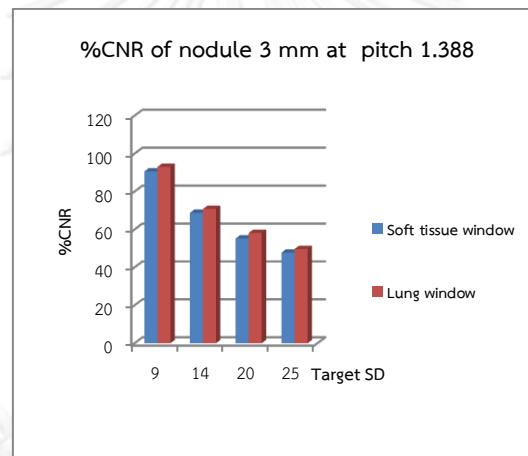
(c)

Figure 4. 24 The percent CNR of nodule 5 mm, at 120 kVp compared between soft tissue window and lung window for pitch 0.637 (a), pitch 0.813 (b) and pitch 1.388 (c)



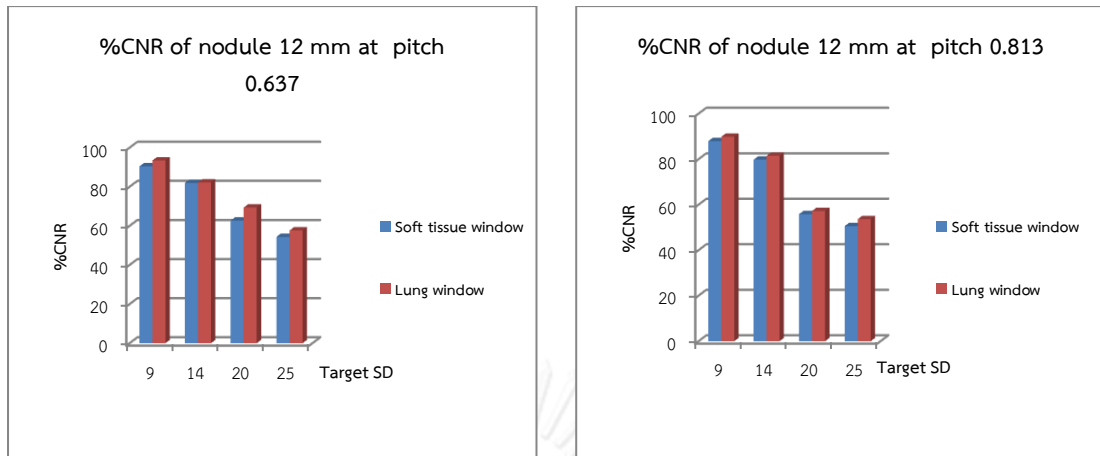
(a)

(b)



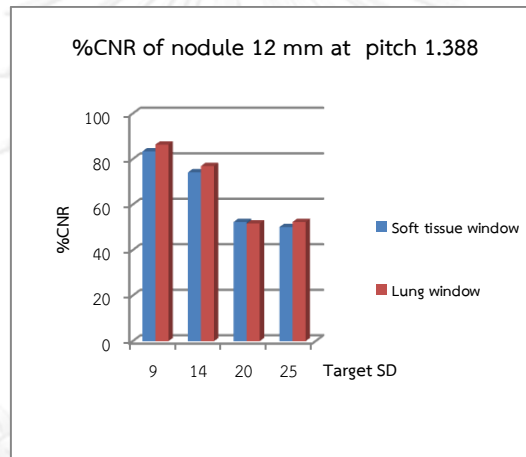
(c)

Figure 4. 25 The percent CNR of nodule 3 mm, at 120 kVp compared between soft tissue window and lung window for pitch 0.637 (a), pitch 0.813 (b) and pitch 1.388 (c)



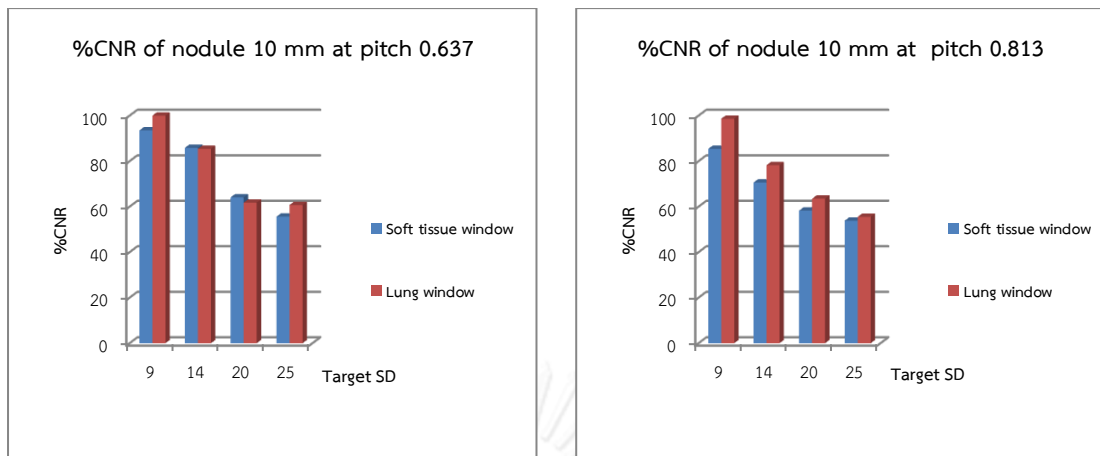
(a)

(b)



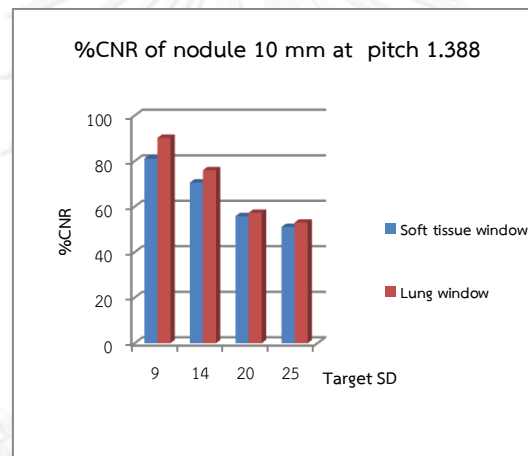
(c)

Figure 4. 26 The percent CNR of nodule 12 mm, at 100 kVp compared between soft tissue window and lung window for pitch 0.637 (a), pitch 0.813 (b) and pitch 1.388 (c)



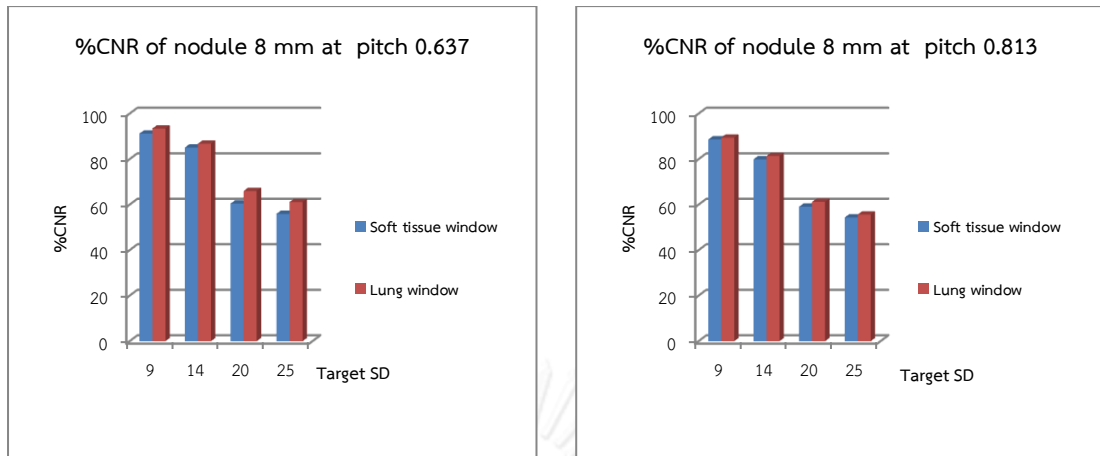
(a)

(b)



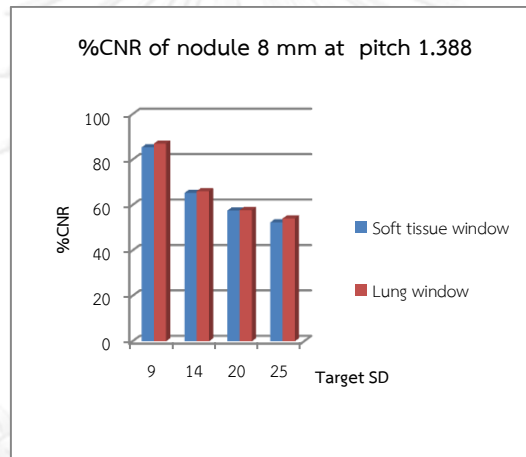
(c)

Figure 4. 27 The percent CNR of nodule 10 mm, at 100 kVp compared between soft tissue window and lung window for pitch 0.637 (a), pitch 0.813 (b) and pitch 1.388 (c)



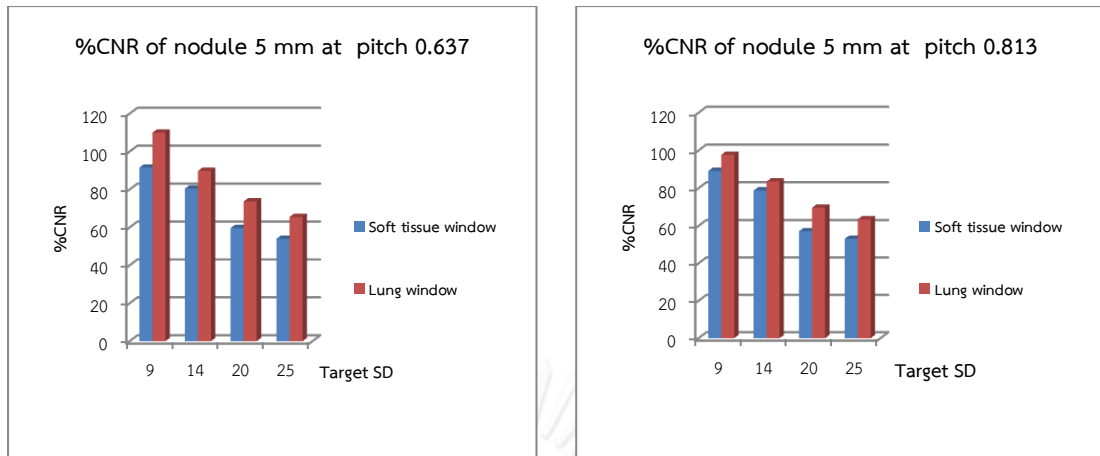
(a)

(b)



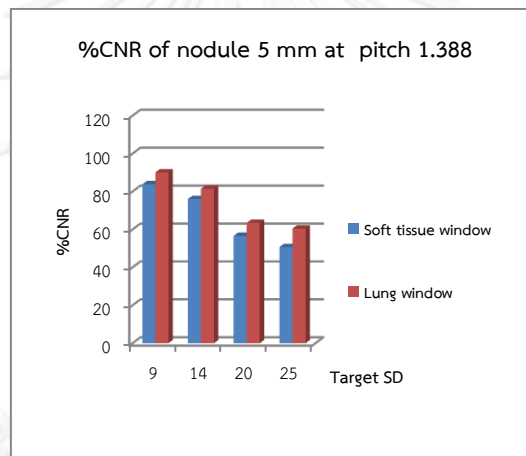
(c)

Figure 4. 28 The percent CNR of nodule 8 mm, at 100 kVp compared between soft tissue window and lung window for pitch 0.637 (a), pitch 0.813 (b) and pitch 1.388 (c)



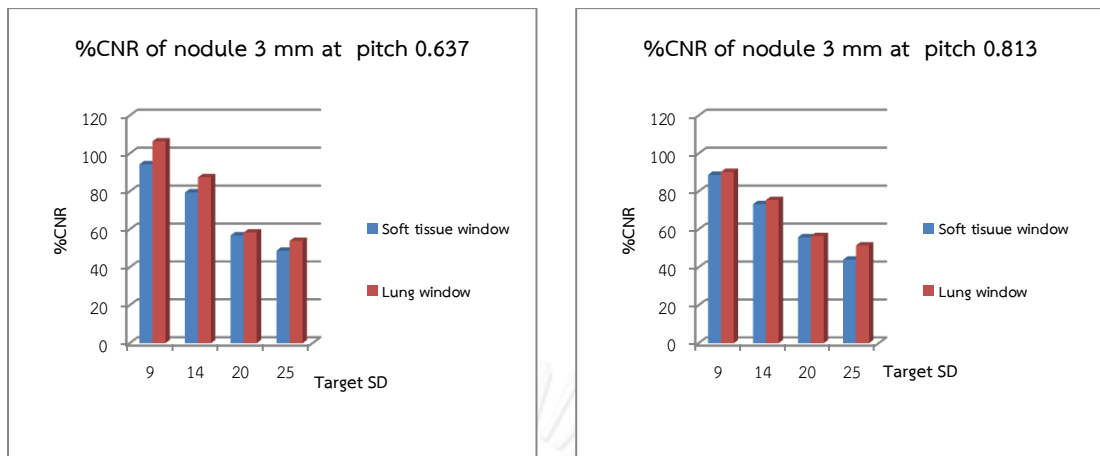
(a)

(b)



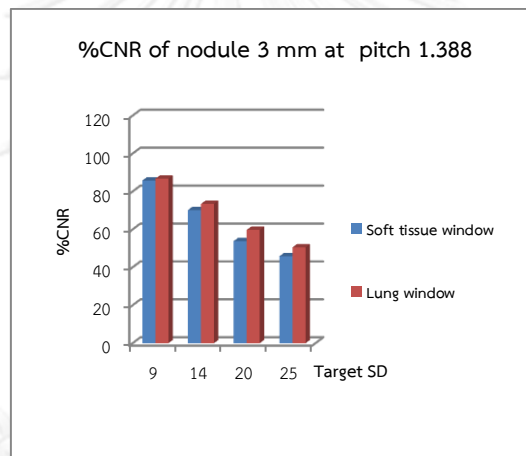
(c)

Figure 4. 29 The percent CNR of nodule 5 mm, at 100 kVp compared between soft tissue window and lung window for pitch 0.637 (a), pitch 0.813 (b) and pitch 1.388 (c)



(a)

(b)



(c)

Figure 4. 30 The percent CNR of nodule 3 mm, at 100 kVp compared between soft tissue window and lung window for pitch 0.637 (a), pitch 0.813 (b) and pitch 1.388 (c)

When compared percent CNR between soft tissue window and lung window, percent CNR of lung window is higher than soft tissue window for both kVp and all pitch.

## 4.5.2 Qualitative image quality

### 4.5.2.1 Image scoring

The agreement of image quality scored by two radiologists was determined by calculating weighted Kappa of the variation the pitch, Target SD and kVp for soft tissue window and lung window as illustrated in Table 4.26 and Table 4.27

Table 4. 26 The image scoring of Lung man chest phantom with soft tissue window

Radiologist B	Radiologist A		Total
	Score 3	Score 4	
Score 3	8	1	9 (37.5%)
Score 4	3	12	15 (62.5%)
Total	11( 45.8%)	13 (54.2%)	24

\*Weighted kappa k-value=0.660

According to the results as in Table 4.26 indicated that a good agreement of the interpretation was obtained from two radiologists (k-value = 0.660).

Table 4. 27 The image scoring of Lung man chest phantom with lung window.

Radiologist B	Radiologist A		Total
	Score 4	Score 5	
Score 4	9	1	10 (41.7%)
Score 5	3	11	14 (58.3%)
Total	12( 50%)	12 (50%)	24

\*Weighted kappa k-value=0.667

The k-value from weighted kappa is usually interpreted the strength of agreement, and the k-value of 0.667 is obtained from this study, which means the strength of agreement is good.

### 4.5.2.2 Spatial resolution

The resolution was assessed by the visualization of the amount of simulated nodules (12, 10, 8, 5 and 3 mm in diameter) with varying pitch, Target SD and kVp on soft tissue



window and lung window. The spatial resolution of standard soft tissue window and lung window is shown in Table 4.28

Table 4. 28 The spatial resolution of Lung man chest phantom at 100 and 120 kVp

kVp	The number of visualized nodules					
	Pitch 0.637		Pitch 0.813		Pitch 1.388	
	S	L	S	L	S	L
100	4	5	4	5	4	5
120	4	5	4	5	4	5

\*S- soft tissue window, L- lung window

Table 4.28 shows number of visualized simulated nodules with varying pitch, Target SD and kVp. The best spatial resolution of 5 simulated nodules was obtained with lung window at both tube potential and all pitch.

## CHAPTER V

### DISCUSSION AND CONCLUSIONS

#### 5.1 Discussion

With technological advances of computed tomography (CT), the development of multi-detector row CT has extremely increased the speed of image acquisition. As the number of detector slice increases, gantry rotation speed increases and spatial resolution improve leading to increasing of radiation dose to the clinical studies of CT. The modern MDCT provides a beneficial function such as automatic tube current modulation to reduce the radiation dose to patient. Furthermore, the user can adjust parameters to modify the image quality relate to the radiation dose. One of the parameters controlled the image quality is Target Standard Deviation (Target SD), a Toshiba specific term. The Target SD is able to adjust the range of tube current by the automatic exposure control (AEC) during gantry rotation to maintain a constant user-specified noise level in the image [2]. In this study, Z-axis modulation has been applied to provide the high efficiency of the radiation dose reduction and maintain image quality at the optimal Target SD for the acceptable image quality and radiation dose.

##### 5.1.1 Measurement of CTDI

Quality control of CT system is very important and should be firstly performed before research data collection. The results of dose measurement are verified for accuracy and reproducibility. All the measured CT Dose was evaluated following the IAEA Human Health No.19 protocol.

$C_{a,100}$  in air was measured using head and body protocols in all kVp and slice collimation.  $C_{a,100}$  values decreases when slice collimation increases. In each slice collimation when kVp increases from 80 kVp to 135 kVp results in  $C_{a,100}$  values increases for both head and body protocols.  $C_{VOL}$  displayed on the CT monitor was verified by the comparison of the measurements and IEC values at the same kVp, mAs and slice collimation. The measured  $C_{VOL}$  in body phantom were greater than 10% of the IEC values. The discrepancy between the measurement and the IEC values result from the uncertainty of chamber position, chamber type and measurement scenario such as the precision of reading, tube loading, the phantom construction, over scan phenomenon, the chamber response in phantoms and the inaccuracy on laser beam alignment[21].

##### 5.1.2 Radiation dose, pitch and Target SD

The relationship between  $C_{VOL}$  and Target SD, for the increasing of Target SD from 9 to 25 and pitch from 0.637 to 1.388 results in  $C_{VOL}$  decreased as shown in Table 4.14 and Table 4.15

When compared  $C_{VOL}$  between 120 kVp and 100 kVp, at Target SD 9 and 14, the  $C_{VOL}$  at 120 kVp is slightly higher than 100 kVp in all pitch. At Target SD 20 and 25,  $C_{VOL}$  did not change in all pitch, but result in increased noise. Thus, MDCT (in terms of tube current modulation) automatically increases mAs to compensate the signals [1]. Mahesh et al[22] studied the relationship between dose and pitch for a particular MDCT scanner and concluded that when the pitch is increased, a proportionate increase in tube current is automatically made to maintain similar noise conditions in the image. In contrast, when increasing pitch the patient dose is proportionately reduced on a single-slice helical scanner when other parameters are held constant.  $C_{VOL}$  of lowest pitch 0.637 was higher than  $C_{VOL}$  at pitch 0.813 and Target SD 9 for both kVp because the small pitch provides high radiation dose due to high overlapping data acquisition.

The small focus was set at all scans except at pitch 1.388 on Target SD 9, so the  $C_{VOL}$  is higher than the other pitch because the switching from the small focus to the large focus is automatically adjusted at kVp 120 , mA 200 and kVp 100, mA 240 . Thus, the results of the greater area of the large focus yields an increased photon flux[23].

According to the AEC system at mA range 10-400 in this study, in the CT images, in lateral and AP diameters were measured at the tip of the xiphoid and the area of the cross section of an ellipsis calculated with indicative Target SD to estimate the tube current [24]. Therefore, the factor affecting on radiation dose are Target SD and kVp.

When Target SD increased results in the radiation dose decreased. Blobel, J et al[24] studied the optimization and reduction of CT radiation exposure using Sure Exposure control, illustrated by a thoracic protocol and concluded that Target SD at 10, 12.5 and 15 yield 25%, 30% and nearly 50% respectively in radiation dose reduction. However their study investigated in the 16 MDCT, but our study investigated in 320 MDCT and Matsumoto, K et al [16] reported that a targeted SD of 150 were to be used for nodule identification with the low-dose CT protocol using AEC and the radiation dose could be reduced by almost 75%. Their study performed in the 64 MDCT.

### **5.1.2.1 The assessment of image quality**

#### **5.1.2.1.1 Contrast to Noise Ratio**

In order to eradicate the variance from the nodules location, the CNRs were grouped of the simulated nodules of 12, 10, 8, 5 and 3 mm in diameter respectively. Target SD 9 with pitch 0.813 was the baseline for normalized percent CNR due to the expected lowest noise level.

Pitch 0.637 presented the highest percent CNR compared to other pitch for all nodule sizes and Target SD at both kVp because the low pitch provides low image noise. The percent CNR reduced from 55 to 50% when increased Target SD from 9 to 25 for all nodule sizes. The percent CNR of 120 kVp is higher than 100 kVp for all Target SD and pitch because higher kVp increases more photons reaching the detectors. Therefore, the factors affecting on CNR are Target SD, pitch and kVp.

However, large variation in percent CNR of small size nodules especially nodules size 5 and 3 mm diameters were observed. The main variable factors result from the unstable sites of circular ROI on a very small size nodule. This also affected to variation of mean CT number of nodule and the standard deviation value of the background.

The percent CNR of lung window is higher than soft tissue window on both kVp because the window width and level range of lung window (-600 to 1600) is wider than soft tissue window (60 to 360) and clearly visible edge of nodule, thus when placed the circular ROI on lung window, it is high accuracy.

#### **5.1.2.1.2 The assessment of qualitative image quality**

Image quality was evaluated by two radiologists for soft tissue window and lung window. The soft tissue window provides the best image quality in all Target SD, pitch and kVp. The pitch 1.388 showed the worst score. Total score of 12 was the highest agreement for soft tissue window, while the score of 11 was the highest agreement of image score for lung window. The agreement of kappa value of two radiologists for both window was good ( $k=0.66$ ).

The spatial resolution was considered from the visualization of smallest simulated nodules. The best spatial resolution image was obtained with lung window for both kVp for the clearly visible edge of nodule is on lung window and AEC system is an attempt to maintain image quality.

#### **5.1.2.2 Optimization of radiation dose, image quality, Target SD and pitch**

The lung nodules that have clinical significant are non- calcified nodules (30-40 HU) and ground glass nodules (less than 30 HU) [25]. However, these CT numbers are much lower than CT number of simulated nodule used in this study. The CT number of simulated nodules designed by manufacturer of lung man chest phantom is 100 HU which represent calcified nodule. This is the limitation of this study.

Due to a lower CT number of ground glass nodules, noise made more difficult in lesion detection and the visibility of ground glass nodules can be missed[25]. Thus, it should be concerned when higher Target SD and low tube current had been used.

Optimization protocols should be set up for the benefit of patients according the clinical requirements. The correlation of the radiation dose and image quality was determined using lung man phantom to obtain to optimal protocols for CT chest with the appropriate Target SD according to the pitch and kVp by consider the lowest  $C_{VOL}$  with acceptable image quality.

For routine chest CT, the mediastinum should be reconstructed using pitch number less than 1 with high kVp for multislice CT. Therefore they are suitable for routine chest interpretation [7]. Using Target SD 20, pitch 0.813 and 120 kVp provided radiation dose equal 1.1 mGy, percent CNR is 61.81% with the same agreement interpretation of two radiologists. Although, the percent CNR reduced to 61.81%, the simulated nodules can be detected by two radiologists. Thus, this protocol can be used as optimize protocol for routine chest CT as shown in Figure 5.2

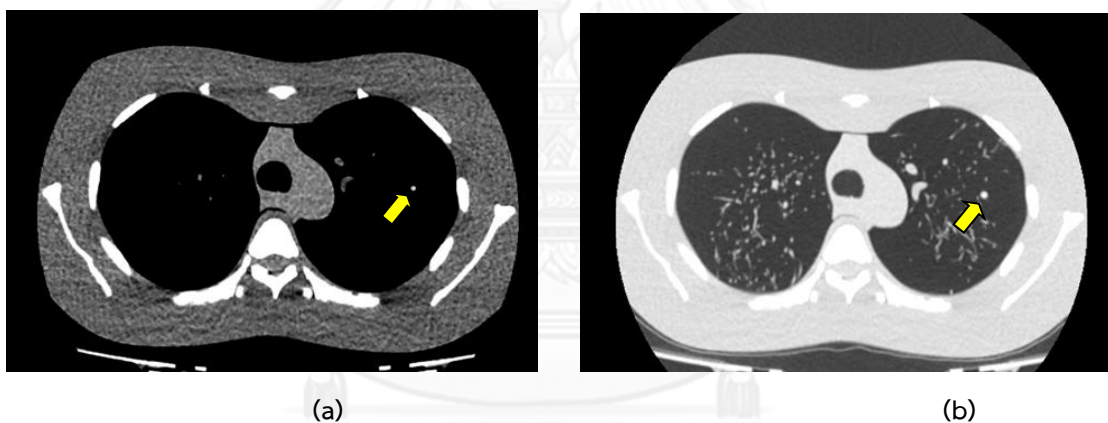


Figure 5. 1 The chest CT with 5 mm nodule with soft tissue window (a) and lung window (b), Target SD 20, 10-400 mA, pitch 0.813 and 120 kVp

According to fixed location of simulated nodules of all scans, two radiologists can recognize the location of simulated nodules. Thus, this is another limitation.

## 5.2 Conclusions

Automatic exposure control is the selected method for radiation dose reduction, while Target SD and kVp are factors affecting the radiation dose. When Target SD increases from 9 to 25, the radiation dose decreases from 5.9 to 0.7 mGy for 120 kVp, and from 5.8 to 0.8 for 100 kVp in lung man phantom study. The factors affecting to image quality are Target SD, pitch and kVp. The optimal Target SD depends on the clinical applications. Target SD of 20 at 10-400 mA, 120 kVp and pitch 0.813 on nodule size 5 mm in diameter is the optimal protocol for routine chest CT.



## REFERENCES

- [1]. Kubo, T., et al. Radiation dose reduction in chest CT: a review. AJR Am J Roentgenol 190 (2008): 335-43.
- [2]. Lee, C.H., et al. Radiation dose modulation techniques in the multidetector CT era: from basics to practice. Radiographics 28 (2008): 1451-9.
- [3]. Kalra, M.K., et al. Techniques and applications of automatic tube current modulation for CT. Radiology 233 (2004): 649-57.
- [4]. Introduction to CT physics [online]. 2004. Available from: [http://www.angelfire.com/nd/hussainpassu/Physics\\_of\\_Computed\\_Tomography.pdf](http://www.angelfire.com/nd/hussainpassu/Physics_of_Computed_Tomography.pdf) [2013, September 22].
- [5]. Ulzheimer, S. and Flohr, T. Multislice CT: Current Technology and Future Developments. In Reiser, M.F., Becker, C.R., Nikolaou, K., Glazer, G. (eds). Multislice CT 3-23. 1 ed: Springer Berlin Heidelberg, 2009.
- [6]. Mahesh, M. The AAPM/RSNA Physics Tutorial for Residents Search for Isotropic Resolution in CT from Conventional through Multiple-Row Detector. Radiographics 22 (2002): 949-62.
- [7]. Prokoba, M. Principles of CT, spiral CT and multislice of CT. In Prokoba, M., Galanski, M. (eds). Spiral and multislice computed tomography of the body 1-36. 1 ed: Thieme, 2003.
- [8]. AAPM REPORT NO 96. The measurement, reporting and management of radiation dose in CT. DEFINITIONS OF QUANTITIES FOR ASSESSING DOSE IN CT: CTDI, CTDIFDA, CTDI100, CTDIW, CTDIVOL, DLP, E: American Association of Physicists in Medicine; 2008. p. 6-11.
- [9]. Goldman, L.W. Principles of CT: radiation dose and image quality. J Nucl Med Technol 35 (2007): 213-25; quiz 26-8.
- [10]. Physics:CT4 [online] 2012. Available from: <http://www.cram.com/flashcards/physics-ct-4-2057025v> [2013, September 24].
- [11]. Primak, A.N., McCollough, C.H. and Bruesewitz, M.R. Relationship between noise, dose, and pitch in cardiac multi-detector row CT. Radiographics 26 (2006): 1785-94.
- [12]. Reddinger, W. CT image quality 1998. Available from: <https://www.yumpu.com/en/document/view/2719502/ct-image-quality-wil-reddinger-msc-rtrct> [2013, October 12].
- [13]. ImPACT Group. Multislice CT scanners CEP08007. Medical Physics Department, Tooting London 2009.

- [14]. Lee, E.J., Lee, S.K., Agid, R., Howard, P., Bae, J.M. andterBrugge, K. Comparison of image quality and radiation dose between fixed tube current and combined automatic tube current modulation in craniocervical CT angiography. AJR Am J Roentgenol 30 (2009): 1754-9.
- [15]. McCollough, C.H., Bruesewitz, M.R. andKofler, J.M. CT Dose Reduction and Dose Management Tools: Overview of Available Options. Radiographics 26 (2006): 503-12.
- [16]. Matsumoto, K., et al. 3D automatic exposure control for 64-detector row CT: radiation dose reduction in chest phantom study. Eur J Radiol 77 (2011): 522-7.
- [17]. Ohno, Y., et al. Influence of detector collimation and beam pitch for identification and image quality of ground-glass attenuation and nodules on 16- and 64-detector row CT systems: experimental study using chest phantom. Eur J Radiol 64 (2007): 406-13.
- [18]. Silverman, J.D., Paul, N.S. andSiewerdsen, J.H. Investigation of lung nodule detectability in low-dose 320-slice computed tomography. Medical Physics 36 (2009): 1700.
- [19]. Verdun, F.R., Denys, A., Valley, J.F., Schnyder, P. andMeuli, R.A. Detection of low-contrast objects: experimental comparison of single- and multi-detector row CT with a phantom. Radiology 223 (2002): 426-31.
- [20]. IAEA. Quality Assurance program for Computed Tomography: Diagnostic and therapy Application. IAEA Human Health Series No 19. Veinna,: IAEA Publishing Section; 2012.
- [21]. IAEA. Dosimetry in Diagnostic Radiology: An International Code of Practice TRS No 457. Veinna: IAEA Publishing Section; 2007.
- [22]. Mahesh, M., Scatarige, J.C., Cooper, J. andFishman, E.K. Dose and pitch relationship for a particular multislice CT scanner. AJR Am J Roentgenol 177 (2001): 1273-5.
- [23]. Hamberg, L.M., Rhea, J.T., Hunter, G.J. andThrall, J.H. Multi-detector row CT: radiation dose characteristics. Radiology 226 (2003): 762-72.
- [24]. Blobel, J., Mews, J., De, V.H., Juran, R. andRogalla, P. Optimization and Reduction of CT Radition Exposure using SureExposure control, illustrated by a thorax protocol [online]. 2004. Available from: [http://www.european-hospital.com/media/article/2161/Optimization\\_and\\_Reduction\\_of\\_CT\\_6\\_2004.pdf](http://www.european-hospital.com/media/article/2161/Optimization_and_Reduction_of_CT_6_2004.pdf) [2013, October 25].



- [25]. Funama, Y., et al. Detection of Nodules Showing Ground-Glass Opacity in the Lungs at Low-Dose Multidetector Computed Tomography: Phantom and Clinical Study. J Comput Assist Tomogr 33 (2009): 49-53.





APPENDICES

จุฬาลงกรณ์มหาวิทยาลัย  
**CHULALONGKORN UNIVERSITY**

## Appendix A: Data record form

Radiation dose

No. of series	Name of protocol ( Pitch/Target SD)	kVp	C <sub>vol</sub> (mGy)	DLP (mGy.cm)
1	0.637/ 9 (1)	120		
2	0.637/ 9 (2)	120		
3	0.637/ 9 (3)	120		
4	0.637/ 9 (1)	100		
5	0.637/ 9 (2)	100		
6	0.637/ 9 (3)	100		
7	0.637/14 (1)	120		
8	0.637/14 (2)	120		
9	0.637/14 (3)	120		
10	0.637/14 (1)	100		
11	0.637/14 (2)	100		
12	0.637/14 (3)	100		
13	0.637/ 20 (1)	120		
14	0.637/ 20 (2)	120		
15	0.637/ 20 (3)	120		
16	0.637/ 20 (1)	100		
17	0.637/ 20 (2)	100		
18	0.637/ 20 (3)	100		
19	0.637/ 25 (1)	120		
20	0.637/ 25 (2)	120		
21	0.637/ 25 (3)	120		
22	0.637/ 25 (1)	100		
23	0.637/ 25 (2)	100		
24	0.637/ 25 (3)	100		
25	0.813/ 9 (1)	120		
26	0.813/ 9 (2)	120		
27	0.813/ 9 (3)	120		
28	0.813/ 9 (1)	100		
29	0.813/ 9 (2)	100		
30	0.813/ 9 (3)	100		
31	0.813/14 (1)	120		
32	0.813/14 (2)	120		
33	0.813/14 (3)	120		
34	0.813/14 (1)	100		
35	0.813/14 (2)	100		

CT number measurement

No. of series	Name of protocol ( Pitch/Target SD)	kVp	Nodule size (mm)		
			CT number (nodule)	CT number (background)	SD (background)
1	0.637/ 9 (1)	120			
2	0.637/ 9 (2)	120			
3	0.637/ 9 (3)	120			
4	0.637/ 9 (1)	100			
5	0.637/ 9 (2)	100			
6	0.637/ 9 (3)	100			
7	0.637/14 (1)	120			
8	0.637/14 (2)	120			
9	0.637/14 (3)	120			
10	0.637/14 (1)	100			
11	0.637/14 (2)	100			
12	0.637/14 (3)	100			
13	0.637/ 20 (1)	120			
14	0.637/ 20 (2)	120			
15	0.637/ 20 (3)	120			
16	0.637/ 20 (1)	100			
17	0.637/ 20 (2)	100			
18	0.637/ 20 (3)	100			
19	0.637/ 25 (1)	120			
20	0.637/ 25 (2)	120			
21	0.637/ 25 (3)	120			
22	0.637/ 25 (1)	100			
23	0.637/ 25 (2)	100			
24	0.637/ 25 (3)	100			
25	0.813/ 9 (1)	120			
26	0.813/ 9 (2)	120			
27	0.813/ 9 (3)	120			
28	0.813/ 9 (1)	100			
29	0.813/ 9 (2)	100			
30	0.813/ 9 (3)	100			
31	0.813/14 (1)	120			
32	0.813/14 (2)	120			
33	0.813/14 (3)	120			
34	0.813/14 (1)	100			
35	0.813/14 (2)	100			

Image quality Scoring

No. of series	Score				
	1	2	3	4	5
1					
2					
3					
4					
5					
6					
7					
8					
9					
10					
11					
12					
13					
14					
15					
16					
17					
18					
19					
20					
21					
22					
23					
24					

- 1 Visualize blur of all simulated nodules.
- 2 Visualize 12 mm. in diameter of simulated nodule with sharp edge or partly visualize 10 mm. in diameter of simulated nodules.
- 3 Visualize 8 and 10 mm. in diameter of simulated nodule with sharp edge or partly visualize 5 mm. in diameter of simulated nodule.

Image quality Scoring (Cont.)

- 4 Visualize 5mm. in diameter of simulated nodule with sharp edge or partly visualize 3 mm. in diameter of simulated nodule.
- 5 Visualize all simulated nodules with sharp edge.



## Appendix B: Quality Control of MDCT system

### 1. Scan Localization Light Accuracy

**Purpose:** To test congruency of scan localization light and scan plane.

**Method:** Tape localization film to the backing plate making sure that the edges of the film are parallel to the plate edges. Place the film vertically along the midline of the couch aligned with its longitudinal axis. Raise the table to the head position. Make both internal and external light with unique pin pricks along the midline of the light. Expose the internal light localization using the narrowest slice setting at 120-135 kVp, 50-100 mAs. For external light, increment table to light position under software control and expose the film.

**Tolerance:** The center of the irradiation field from the pin pricks should be less than 2 mm

#### Results:

Measured Deviation External ....0...mm

Internal .....1...mm

**Comment:** Pass

### 2. Alignment of table to gantry

**Purpose:** To verify the long axis of the table is horizontally aligned with a vertical line passing through the rotational axis of the scanner

**Method:** Locate the table midline using a ruler and mark it on a tape affixed to the table. With the gantry untilted, extend the table top into gantry to tape position. Measure the horizontal deviation between the gantry aperture center and the table midline.

**Tolerance:** The Deviation should be within 5 mm

Results:

Table B 1: Alignment of table and bore

	Table	Bore
Distance from Right to Centre (mm)	234	361
Distance from Centre to Left (mm)	234	359
Measured Deviation* (mm)	0	1

\*Measured deviation = (Distance from right to center – Distance from center to Left)/2

Comment: Pass

### 3. Table increment Accuracy

**Purpose:** To assess accuracy and reproducibility of table longitudinal motion.

**Method:** Tape a measuring tape at the foot end of the table. Place a paper clip at the center of the tape to function as an indicator. From the initial position move the table 300, 400 and 500 mm into the gantry under software control. Record the relative displacement of the pointer on the ruler. Reverse the direction of motion and repeat.

**Tolerance:** Positional errors should be less than 3 mm at 300 mm position.

Results:

Table B 2: Table increment Accuracy

Indicated (mm)	Measured (mm)	Deviation (mm)
300	300	0
400	400	0
500	500	0
-300	-300	0
-400	-400	0
-500	-499.85	0.15



*\*Deviation = | Indicated – Measured|*

**Comment:** Pass

#### 4. Slice increment Accuracy

**Purpose:** To assess the accuracy of the slice increment.

**Method:** Set up as you would for beam profile measurement. Choose 120 kVp, 100 mAs and smallest slit width. Perform several scans with different programmed slice separations under auto control. Scan the film with a densitometer and measure the distance between the peaks.

**Tolerance:** Positional errors should be less than 3 mm at 300 mm position.

**Results:**

Table B 3: The accuracy of slice separation

Slice Separation in mm	Measured Separation in mm	Deviation (mm)
20	20	0
30	30	0
50	50	0

*\*Deviation = |Slice separation – Measured separation|*

**Comment:** Pass

#### 5. Gantry angle tilt

**Purpose:** To assess the limit of gantry tilt and the accuracy of tilt angle indicator

**Method:** Tape a localization film to the backing plate making sure that the edges of the film are parallel to the edges of the backing plate. Place the film vertically along the midline of the couch aligned with its longitudinal axis. Raise the table to the head position. Move the table into the gantry. Center plate to the laser alignment light. Expose the film at inner light location using narrowest slit, 120-135 kVp, 50-100 mAs. Tilt the gantry to one extreme from the console. Record the indicated gantry angle. Expose the film using the above technique. Measure

the clearance from the closest point of gantry to midline of the table. Tilt the gantry to its extreme in the opposite direction. Record clearance and repeat the exposure. Measure the tilt angles from the images on the film.

**Tolerance:** Deviation between indicated and measured tilt angles  $\leq 3^\circ$  and Gantry clearance should be  $\geq 30$

Results:

Table B 4: The accuracy of gantry angle tilt

	Away	Toward
Indicated angle	22°	22°
Measured angle	22°	22°
Deviation*	0	0
Clearance (cm.)	33	33

\*Deviation =  $|$ Indicated angle – Measured angle $|$

**Comment:** Pass

#### 6. Reproducibility of C.T. Numbers.

**Method:** Slice thickness of 10 mm was used, which one scan using typical head technique, obtains four scans. The same ROI as position dependence in location 5 was used, which is the center of the phantom, measure mean C.T. numbers for each of the four scans.

**Tolerance:** The coefficient of variation of mean C.T. numbers of the four scans should be less than 0.002

Results:

Table B 5: Reproducibility of CT Number

Run Number	1	2	3	4
Mean C.T. (HU)	118.35	118.18	118.08	118.34

Mean Global CT number	118.24
Standard Deviation	0.13
Coefficient of Variation	0.001

**Comment:** Pass

### 7. mAs Linearity

**Method:** Position of the the C.T. dose head phantom centered in the gantry and insert 10 cm long pencil chamber in the center slot of the phantom. Choose the same kVp and time as used for head scan. Obtain four scans in each of the mA stations usually used in the clinic. For each mA station record the exposure in mGy for each scan. Scans should be performed in the increasing order of mA. Calculate mGy/mAs for each mA setting.

**Technique:** 120 kVp, 1.0 s, varying mA, FOV 240 mm

**Results:**

Table B 6: mGy and mAs linearity

mA	Exposure in mGy				mGy/mAs	C.V
	Run1	Run2	Run3	Run4		
50	0.499	0.500	0.499	0.494	0.01	-
100	0.993	0.990	0.998	0.997	0.01	0.001
200	1.999	1.975	1.995	1.999	0.01	0.001
250	2.509	2.493	2.504	2.474	0.01	0.001
300	3.835	3.796	3.382	3.835	0.01	0.122
400	5.094	5.117	5.101	5.085	0.01	0
500	6.319	6.292	6.323	6.311	0.01	0.005

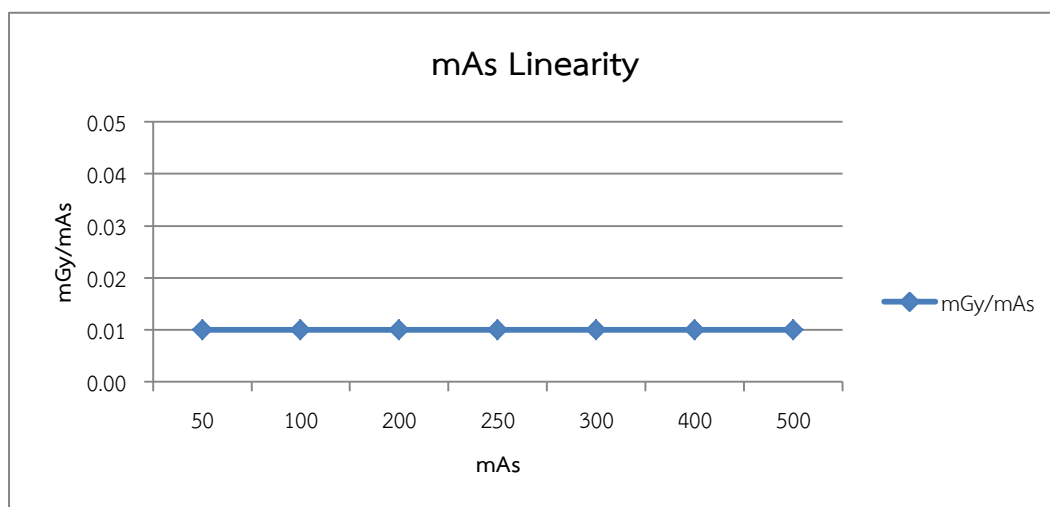


Figure B 1 The relationship of mGy/mAs and mAs

**Comment:** Pass

#### 8. Linearity Of C.T. Numbers

**Method:** The Catphan phantom as described in beam alignment was set up. Choose the section containing the test objects of different C.T. numbers. Choose the head technique and perform a single transverse scan. Choose a region of interest (ROI) of suitable size to cover the test objects. Place the ROI in the middle of each test object and record the mean C.T. number.

**Technique:** 120 kVp 300 mA 1.0 s, FOV 240 mm, Slice thickness 8 mm

**Tolerance:** R-square between measured CT number and linear attenuation coefficient ( $\mu$ ) more than 0.9

**Results:**

Table B 7: Linearity of CT Number

Material	Expected CT no.(HU)	Measured CT no.(HU)	$\mu$ [ $\text{cm}^{-1}$ ]
Air (Superior)	-1000	-1007.9	0
Air (Inferior)	-1000	-1008.3	0
PMP	-200	-193.9	0.188
LDPE	-100	-106.1	0.209
Polystyrene	-35	-35.6	0.229
Acrylic	120	113.9	0.277
Delrin™	340	348.7	0.344
Teflon	990	1011.9	0.572

**Note** Expected C.T. numbers are either the predicted ones or the ones obtained during the previous annual measurement.

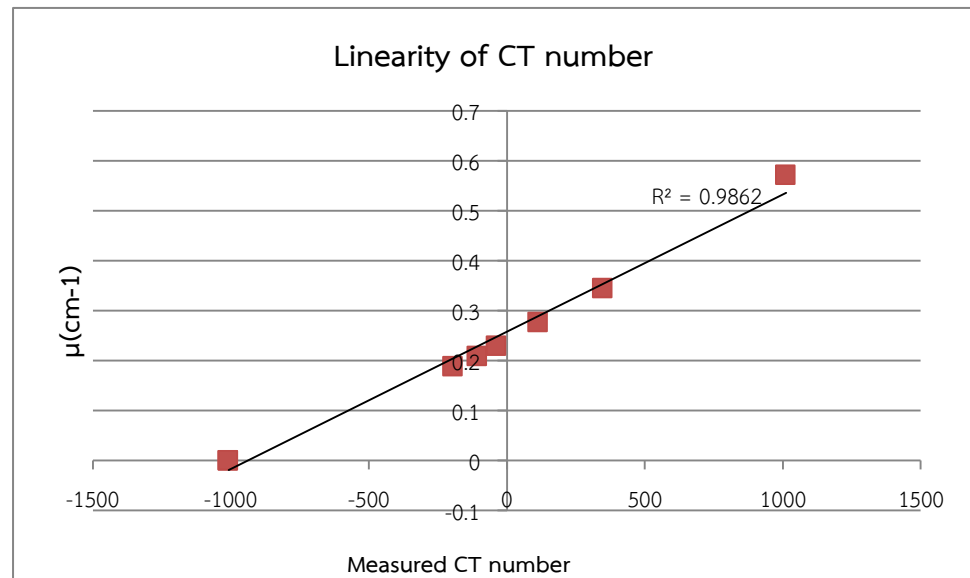


Figure B 2 Linearity of CT number

**Comment:** Pass

### 9. Accuracy of Distance Measurement

**Purpose:** To test accuracy of Distance Measurement and for circular symmetry of the CT image

**Method:** The Catphan phantom as described in beam alignment was set up. Choose the section containing the test accuracy of distance measurement. Choose the head technique and perform a single transverse scan. Measured object in x and y axis.

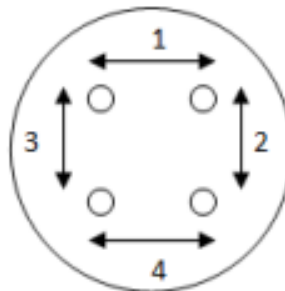


Figure B 3 Distance accuracy

Results:

Table B 8: Accuracy of Distance Measurement

Position	Indicated (mm)	Measured (mm)	Difference (mm)
1	50	49.80	0.20
2	50	49.70	0.30
3	50	50.20	0.20
4	50	49.80	0.20

$$\text{Difference} = |\text{Indicated} - \text{Measured}|$$

**Comment:** Pass

#### 10. High Contrast Resolution

**Purpose:** To test resolution sections ranging from 1 to 21 lines pairs per cm. This radial design pattern eradicates the possibility of streaking artifacts from other test objects.

**Method:** The Catphan phantom as described in beam alignment was set up. Choose the section containing the high resolution test objects (CTP528, 21 line pair high resolution Module). Choose the head technique and perform a single axial scan. Choose the area including the high resolution test objects and magnify as necessary. Choose appropriate window and level for the best visualization of the test objects. Record the smallest test object visualized on the monitor.

**Technique:** 120kVp, 300mA, 1.0 s, FOV 240 mm

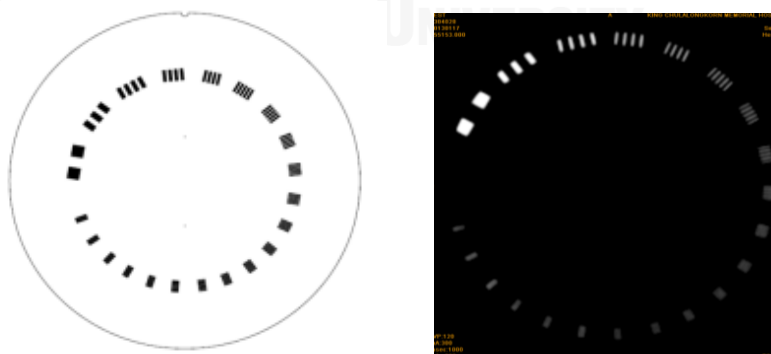


Figure B 4 High contrast resolution

Results:

Table B 9: High contrast resolution

Slice Thickness in mm	Resolution (lp/cm)
8	7 (0.071 mm)

Comment: Pass

### 11. Low Contrast Resolution

**Purpose:** To assess the actual target contrasts before testing specific contrast performance specifications.

**Method:** The Catphan phantom as described in beam alignment was set up. Choose the section containing the low resolution test objects (CTP515 Sub-slice and supra-slice low contrast Module). Choose the head technique. Perform a single transverse scan. Choose the area including the high resolution test objects and magnify as necessary. Choose appropriate window and level for the best visualization of the test objects. Record the smallest test object visualized.

**Technique:** 120 kVp, 300 mA, 1.0 s, FOV 240 mm slice collimation 8 mm

**Tolerance:** should see 4 spokes at Supra- slice 0.5% nominal target contrast level

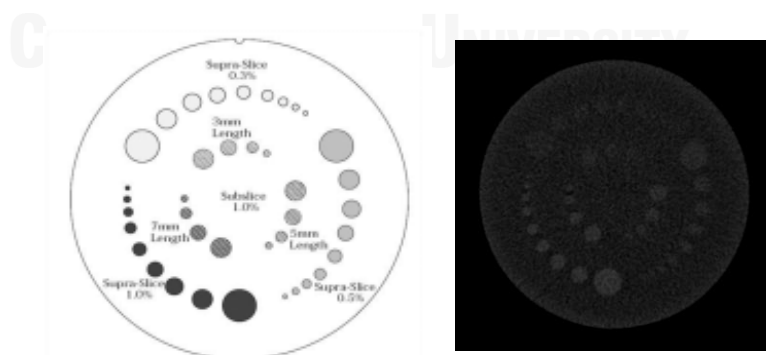


Figure B 5 Low contrast detectability

Results:

Table B 10: Low contrast detectability

Supra-slice	Nominal target contrast level	spokes
	0.3%	4
	0.5%	7
	1%	8.5
Sub-slice	Nominal target contrast level	spokes
	3 mm Length	3
	5 mm Length	3.5
	7 mm Length	4

Comment: Pass

## 12. Slice Thickness Accuracy

**Purpose:** To assess the accuracy of the slice thickness.

**Method:** The Catphan phantom as described in beam alignment was set up as you would for beam profile measurement. Choose the section containing the accuracy of the slice thickness test objects (CTP404 slice width Module). Choose the head technique. Choose 120 Kvp, 300 mAs, smallest slit width. Perform several scans with different programmed slice thicknesses under auto control. Perform scan following Catphan manual in each slice collimation. Calculate the real slice thickness.

**Technique:** 120kVp, 300mA, 1.0s, FOV 240 mm

**Tolerance:** The deviation should be less than 1

Results:

Table B 11: Slice thickness accuracy

Slice thickness in mm	Measured thickness in mm	Deviation
2	2.52	0.52
4	3.82	0.18
8	8.02	0.02

\*Deviation =  $| \text{Slice thickness} - \text{Measured thickness} |$



Comment: Pass

### 13. Image Uniformity

**Method:** The Catphan phantom as described in beam alignment was set up. Choose the CTP 486 section (Solid image uniformity module). Choose the head technique and perform a single transverse scan. Choose a region of interest (ROI) of sufficient size to cover the test objects. Place the ROI in the middle of each test object and record the mean C.T. number.

**Technique:** 120kVp, 300mA, 1.0s, FOV 240 mm, Slice thickness 8 mm

**Tolerance:** Difference should be less than 5 HU

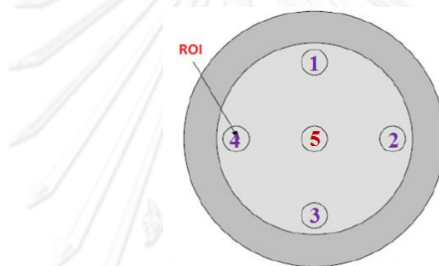


Figure B 6 Image Uniformity

Results:

Table B 12: Image Uniformity

Position	CT number (HU)	SD	Difference (HU)
Center	2.40	2.50	0
1	3.00	2.20	0.60
2	2.60	2.10	0.20
3	2.30	2.30	0.10
4	2.70	2.30	0.30

*\*Difference = |CT number center - CT number peripheral|*

Comment: Pass

## VITA

NAME Miss Chatnapa Nuntue  
DATE OF BIRTH 6 October 1987  
PLACE OF BIRTH Phetchabun, Thailand  
EDUCATION Bachelor of Science  
(Radiological Technology)  
Faculty of Allied Health Science,  
Naresuan University, 2009  
ADDRESS 46/34 M.12 Watsai, Muang,  
Nakhonsawan 60000, Thailand  
E-mail chatnapan@hotmail.com

## ACADEMIC PUBLICATIONS

1. Nuntue, C., Krisanachinda A., Khamwan, K., Tongbai, T. and Hongsmatip, P. Optimization of 320 MDCT using beam pitch and tube current modulation for proper target SD on lung nodule –chest protocol: phantom study. In Proceedings of 13th Asia-Oceania Congress of Medical Physics & 11th South-East Asian Congress of Medical Physics, pp. 109-12. Singapore, 2013.